

Development and Non-Invasive Monitoring of Tissue-Engineered Cardiovascular Implants

Von der Medizinischen Fakultät
der Rheinisch-Westfälischen Technischen Hochschule Aachen
zur Erlangung des akademischen Grades eines Doktors der Theoretischen Medizin
genehmigte Dissertation

vorgelegt von

Saurav Ranjan Mohapatra, M. Sc.

aus

Kendupalli (Indien)

Berichter: Prof. Dr. med. dent. Christian Apel
Univ.-Prof. Dr. med. Fabian Kießling

Tag der mündlichen Prüfung: 08.05.2025

To my teachers

List of publications

Dissertation

S. R. Mohapatra, E. Rama, C. Melcher, T. Call, M. A. Enezy-Ulbrich, A. Pich, C. Apel, F. Kiessling & S. Jockenhoevel: From In Vitro to Perioperative Vascular Tissue Engineering: Shortening Production Time by Traceable Textile-Reinforcement; Tissue Engineering and Re- generative Medicine; 2022, Volume 19. <https://doi.org/10.1007/s13770-022-00482-0>

S. R. Mohapatra, E. Rama, M. P. Werner, T. Call, T. Loewenberg, A. Loewen, C. Apel, F. Kiessling & S. Jockenhoevel: Novel Bioreactor Design for Non-invasive Longitudinal Monitor- ing of Tissue-Engineered Heart Valves in 7T MRI and Ultrasound; Annals of Biomedical Engi- neering; 2024. <https://doi.org/10.1007/s10439-024-03632-8>

D 82 (Diss. RWTH Aachen University, 2025)

Others

E. Rama, **S. R. Mohapatra**, C. Melcher, T. Nolte, S. M. Dadfar, R. Brueck, V. Pathak, A. Rix, T. Gries, V. Schulz, T. Lammers, C. Apel, S. Jockenhoevel, F. Kiessling: Monitoring the Re- modeling of Biohybrid Tissue-Engineered Vascular Grafts by Multimodal Molecular Imaging; Advance Science; 2022, Volume 9. <https://doi.org/10.1002/advs.202105783>

E. Rama, **S. R. Mohapatra**, Y. Sugimura, T. Suzuki, S. Siebert, R. Barmin, J. Hermann, J. Baier, A. Rix, T. Lemainque, S. Koletnik, A. S. Elshafei, R. M. Pallares, S. M. Dadfar, R. H. Tolba, V. Schulz, J. Jankowski, C. Apel, P. Akhyari, S. Jockenhoevel, F. Kiessling: In Vitro and in Vivo Evaluation of Biohybrid Tissue-Engineered Vascular Grafts with Transformative ¹H/¹⁹F MRI Traceable Scaffold; Biomaterials; 2024, Volume 311. <https://doi.org/10.1016/j.biomateri- als.2024.122669>



From *In Vitro* to Perioperative Vascular Tissue Engineering: Shortening Production Time by Traceable Textile-Reinforcement

Saurav Ranjan Mohapatra¹ · Elena Rama² · Christoph Melcher³ · Tobias Call¹ ·
Miriam Aischa Al Enezy-Ulbrich⁴ · Andrij Pich⁴ · Christian Apel¹ ·
Fabian Kiessling² · Stefan Jockenhoevel¹

Received: 28 April 2022 / Revised: 18 July 2022 / Accepted: 20 July 2022 / Published online: 6 October 2022
© The Author(s) 2022

Abstract

BACKGROUND: The production of tissue-engineered vascular graft (TEVG) usually involves a prolonged bioreactor cultivation period of up to several weeks to achieve maturation of extracellular matrix and sufficient mechanical strength. Therefore, we aimed to substantially shorten this conditioning time by combining a TEVG textile scaffold with a recently developed copolymer reinforced fibrin gel as a cell carrier. We further implemented our grafts with magnetic resonance imaging (MRI) contrast agents to allow the *in-vitro* monitoring of the TEVG's remodeling process.

METHODS: Biodegradable polylactic-co-glycolic acid (PLGA) was electrospun onto a non-degradable polyvinylidene fluoride scaffold and molded along with copolymer-reinforced fibrin hydrogel and human arterial cells. Mechanical tests on the TEVGs were performed both instantly after molding and 4 days of bioreactor conditioning. The non-invasive *in vitro* monitoring of the PLGA degradation and the novel imaging of fluorinated thermoplastic polyurethane (¹⁹F-TPU) were performed using 7T MRI.

RESULTS: After 4 days of close loop bioreactor conditioning, 617 ± 85 mmHg of burst pressure was achieved, and advanced maturation of extracellular matrix (ECM) was observed by immunohistology, especially in regards to collagen and smooth muscle actin. The suture retention strength (2.24 ± 0.3 N) and axial tensile strength (2.45 ± 0.58 MPa) of the TEVGs achieved higher values than the native arteries used as control. The contrast agents labeling of the TEVGs allowed the monitorability of the PLGA degradation and enabled the visibility of the non-degradable textile component.

CONCLUSION: Here, we present a concept for a novel textile-reinforced TEVG, which is successfully produced in 4 days of bioreactor conditioning, characterized by increased ECM maturation and sufficient mechanical strength. Additionally, the combination of our approach with non-invasive imaging provides further insights into TEVG's clinical application.

Keywords Tissue-engineered vascular grafts · Electrospun scaffolds · Non-invasive monitoring

✉ Stefan Jockenhoevel
jockenhoevel@ame.rwth-aachen.de

¹ Department of Biohybrid and Medical Textiles (BioTex), Center for Biohybrid Medical Systems (CBMS), Institute for Applied Medical Engineering, RWTH Aachen University, Forckenbeckstr. 55, 52074 Aachen, Germany

² Institute for Experimental Molecular Imaging, RWTH Aachen University, Forckenbeckstr. 55, 52074 Aachen, Germany

³ Institute for Textile Technology, RWTH Aachen University, Otto-Blumenthal-Str. 1, 52074 Aachen, Germany

⁴ DWI-Leibniz Institute for Interactive Materials, RWTH Aachen University, Forckenbeckstr. 50, 52074 Aachen, Germany

1 Introduction

Cardiovascular diseases often demand instant care but producing a suitable solution quickly is highly challenging. Replacement of diseased vessels with synthetic grafts or autologous grafts are two main therapy options for these life-threatening conditions. Several polymeric matrices have been developed and studied for use as artificial grafts in vascular applications, including polyurethane (PU), expanded PTFE (ePTFE), and poly(ϵ -caprolactone) (PCL) [1–3]. With the aid of balloons and catheters, vascular bypasses using autografts, artificial grafts, or vascular stents have been widely studied [4–6]. Though clinically established synthetic grafts are currently in use, the indications are limited to higher vascular diameters, and susceptibility to infections can lead to morbidity and mortality [7–9]. In the past few years, tissue engineering has made tremendous advancements, and both *in vitro* and *in vivo* studies have been successfully realized [10]. In combination with polymer scaffolds and autologous cells, tissue engineering has the potential to create body-own replacement structures. Tissue-engineered constructs hold the ability for self-repairing and remodeling [11].

Besides the advancement in vascular tissue engineering, the long *in vitro* culture time remains a big challenge with regard to a successful translation into clinics [12]. It has been reported that TEVGs require two to three months of culture to give a desired implantable condition [13–16]. To serve an acute and subacute case of cardiovascular dysfunction this time is impractical. The conditioning time is given not only to achieve higher cell density but also to bring higher burst strength. An immature extracellular matrix can lead to the development of life-threatening aneurysms in short to medium term [17].

Previous studies have already shown that conditioning the grafts *in vitro* with an oscillating pressure increases the burst pressure over time. However, in those studies, the graft had to be kept in a bioreactor for several weeks to demonstrate suitable mechanical properties for implantation. Gui et al. and Stekelenburg et al. reported a burst pressure of 913.3 ± 150.1 mmHg after 30 days of culture under pulsatile stretching and 903 ± 123 mmHg after 28 days of *in vitro* culture, respectively [18, 19].

Two important factors have to be considered to make a successful TEVG. The first factor that possesses the mechanical stability of the TEVG must imitate the robustness of a native vessel. Second, adhesive and confluent endothelial cells in the lumen area to avoid thrombosis after implantation [20].

We have invented the concept of a textile-reinforced biohybrid vascular graft and, till now, have successfully applied this concept *in vitro* and *in vivo* [21–24]. However,

the current challenge is to reduce the bioreactor conditioning time significantly to foster translation into the clinic. We hypothesize that this could be achieved by either adding an improved textile reinforcement and/or modifying the hydrogel cell carrier. In the present study (Fig. 1), we are employing a non-degradable textile poly(vinylidene fluoride) (PVDF) mesh to give long-term structural support to avoid aneurysm formation. The PVDF textile mesh is coated with an electrospun poly(lactic-co-glycolic-acid) (PLGA) layer to give temporary higher burst strength. The nonwoven PLGA meshes fill up the gaps between textile filaments and introduce microporosity to the graft. The electrospun layer of PLGA has proven to be biocompatible and biodegradable. Apart from that, it is cost-efficient and easily producible [25–27].

Furthermore, we modified the fibrin matrix gel by adding reactive amphiphilic copolymers, which are based on *N*-vinylpyrrolidone (VP). *N*-vinyl lactam-based polymers have been proven biocompatible and possess specific hydration properties [28]. Pich et al. have successfully improved the mechanical properties of fibrin and thrombin-based hydrogels by adding the poly(*N*-vinylpyrrolidone-co-glycidyl methacrylate) (VP-co-GMA) copolymer [29]. We hypothesize that the integration of this copolymer will enhance the initial mechanical strength of the vascular grafts.

Magnetic resonance imaging (MRI) is a non-destructive approach and can be used in both *in vitro* and *in vivo* monitoring. Cardiovascular functions can be broadly investigated by the MRI device because of its optimum contrast of soft tissues [30]. As discussed in a previous study, the incorporation of MRI contrast agents could be exploited as an additional technique to improve vascular grafts' visibility via non-destructive imaging [31]. Non-destructive monitoring of implants provides not only real-time diagnostics but also ensures patient safety. Mertens et al. have successfully shown the enhanced visibility of collagen scaffolds using ultrasmall superparamagnetic iron oxide nanoparticles via 3 T MRI [32]. In addition, Rama et al. have recently shown that after superparamagnetic iron oxide nanoparticles (SPION)-labeling of their vascular grafts' textile scaffold, the longitudinal monitoring of the degradation and remodeling of vascular prostheses is accessible via multimodal imaging [33]. Furthermore, as a valuable alternative to ^1H MRI, Lammers et al. already showed the potential that could result from the employment of highly fluorinated thermoplastic polyurethane (^{19}F -TPU) as a novel material for tissue engineering applications [34]. Indeed, ^{19}F -MRI techniques might provide useful insight, especially for quantitative applications, thanks to the lack of ^{19}F signals in human or animal bodies.

In this study, we present tissue-engineered vascular grafts, which would be ready to be transplanted after only

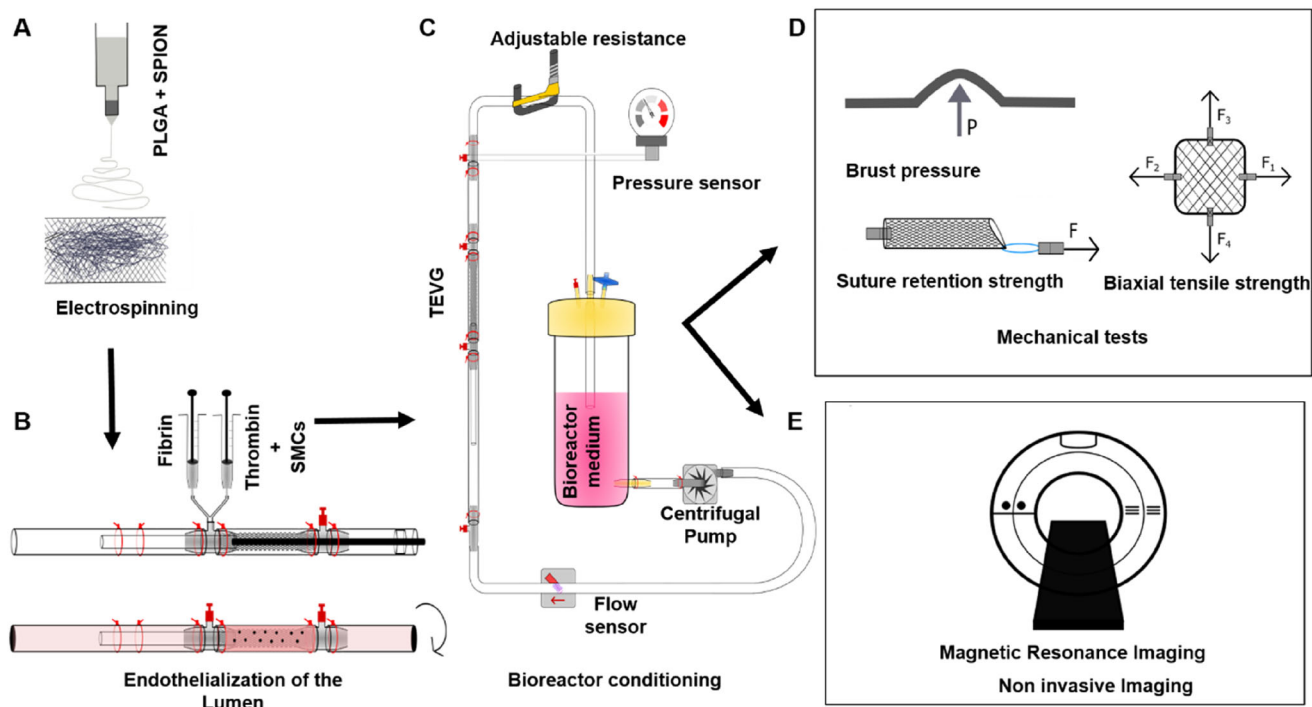


Fig. 1 Schematic representation of the study design. **A** Electrospinning of the PLGA layer on the textile mesh, **B** Molding technique of the TEVG, **C** The closed loop bioreactor, **D** Mechanical tests, **E** Non-invasive Imaging methods

4 days of bioreactor conditioning with well-suited mechanical rigidity to allow implantation. We compared three types of TEVG: (i) *Non-coated TEVG*: contains a not-coated PVDF textile mesh and fibrin matrix hydrogel along with cells (ii) *Coated TEVG*: contains an electrospun PLGA coated PVDF textile mesh and fibrin matrix hydrogel along with cells and (iii) *Copolymer TEVG*: contains VP-co-GMA copolymer along with the coated PVDF textile mesh, fibrin, and cells. The three variants of TEVGs were mechanically tested and histologically analyzed instantly after molding (day 0) and after four days of bioreactor conditioning (day 4). In addition to that, we demonstrate the employment of novel imaging approaches allowing the traceability and monitorability of vascular grafts. Therefore, we aimed to employ non-invasive and non-destructive $^1\text{H}/^{19}\text{F}$ MRI to investigate and monitor our TEVGs' integrity and remodeling. To this end, we also introduced SPION and ^{19}F -TPU into the textile scaffold of our vascular grafts.

2 Materials and methods

2.1 Production of textile mesh

As already described in our previous publication [33], a double-bar Raschel warp-knitting machine (Karl Meyer Holding GmbH & Co. KG, Obertshausen, Germany) was

Table 1 Warp-knitting process parameters for the tubular PVDF mesh structures

Region of the mesh	Chain notation of warp-knitting	EAC value
Brim fibers	0-2-2-2-2-0-2-0-2-2-2-2-0-2// 0-0-2-0-2-0-0-0-0-2-0-2-0-0- 0//	6
Back part	2/2-2-0-2-2-2-4-2-2-0-2-2-2/4//	6
Front part	0-2-2-2-2-2-0-2-0-2-2-2-2-2-0-2//	6

used to produce three different kinds of tubular meshes structures from polyvinylidene fluoride (PVDF) (Lenzing Plastics GmbH & Co. KG, Lenzing, Austria) multifilament fibers (150 dtex, 48 filaments). To alter the inner diameters of the tubular mesh structures, the number of used fibers was varied (4, 6, and 10 fibers). The fabrication parameters and effective arc per centimeter (EAC) value of the warp-knitting process are shown in Table 1.

2.1.1 ^{19}F -TPU fiber fabrication

^{19}F -TPU (Lubrizol, Wickliffe, Ohio, United States) multifilaments were produced via melt spinning (Fourné Polymertechnik GmbH, Alfter, Germany). ^{19}F -TPU pellets were dried at 80 °C for 24 h prior to spinning using a vacuum oven (Thermofischer Scientific, Waltham, MA,

USA). For extrusion of the fibers, extrusion temperatures (T_E) of $T_E = 185\text{--}220\text{ }^\circ\text{C}$ were used. The multifilament spinnerets provided 10 circular shaped capillaries. The spinning line setup consisted of a blow chamber, a mono godget, two godget pairs, a heat channel as well as a winder (SAHM 260XE, Georg Sahn GmbH & Co. KG, Eschwege, Germany) for fiber collection. The heating channel was placed between the two godget pairs and heated to a temperature of $65\text{ }^\circ\text{C}$. VP 3 GA 661/19 (20 vol.-% in deionized water) was used as a spin finish for multifilament fabrication. Multifilaments could be produced at spinning velocities (v_S) of $v_S = 130\text{--}144\text{ m/min}$.

2.2 Electrospinning of SPION-labelled PLGA fibers

Warp-knitted meshes were coated with SPION-labelled PLGA (Purasorb PLG 8523, Corbion Purac Gorinchem, Netherlands) electrospun fibers for 10 min. Therefore, a coaxial spinning head (Bioinicia SL, Paterna, Spain) with a $1400\text{ }\mu\text{m}$ shell capillary and a $580\text{ }\mu\text{m}$ core capillary was used. For each spinning trial, the two used spinning dopes (6 wt% PLGA (shell) and 6 wt% PLGA labeled with 0.2 wt% SPIONs (core), dissolved in methanol (MeOH, neoLab Migge Laborbedarf – Vertriebs GmbH, Heidelberg, Germany) and chloroform (CHCl₃, Carl Roth GmbH & Co. KG, Karlsruhe, Germany) were prepared in a total volume of 10 ml and stirred for 24 h at room temperature until the PLGA was completely dissolved. The SPION solution was added to the core solution directly before execution of the electrospinning process and stirred until reaching a homogenous solution. For coating, the PVDF meshes, 30 cm of the structures were applied on a cylindrical collector. The tip to collector distance was set to 20 cm, and the printing head was driven continuously along the PVDF mesh at a speed of 30 mm/s. The flow rates of the core and shell solutions were set to 0.5 ml/h and 1 ml/h during the spinning process. SPION labeled PLGA fibers were spun at a voltage of + 22 kV (emitter) and – 20 kV (collector). All spinning trials were performed at $25\text{ }^\circ\text{C}$ and 30% humidity.

2.3 Scanning electron microscopy

For microfiber and graft observation, a scanning electron microscope (SEM – 606 LV (JEOL, Tokyo, Japan) was used. The operating voltage was set to 15 kV; images were taken at 100-, 200-, 500- and 1000-fold magnification. To avoid charging effects and ensure electrical conductivity, the specimen was coated with a thin layer of Au/Pt before measuring the SEM images.

2.4 Cell isolation

The human umbilical cord was collected in a transport buffer solution beaker and kept at $4\text{ }^\circ\text{C}$ for 4 h. The umbilical cord was cleaned properly with PBS, and the remaining blood clots were removed. To harvest the smooth muscle cells, the arteries were isolated from the cord and minced into small ring-shaped pieces with a scalpel. The small pieces were distributed horizontally inside a T75 cell culture flask and supplied with a fresh DMEM medium (Thermofischer Scientific).

For the endothelial cells, the lumen of the HU artery was soaked with collagenase (Thermofischer Scientific) for 30 min at $37\text{ }^\circ\text{C}$ for incubation. After the collagenase removal, the cells were cultured in the flask and supplied with an endothelial basal medium (Promocell, Heidelberg, Germany). The umbilical cord was collected from the Gynecology Department at the University Hospital Aachen in accordance with the human subjects' approval of the ethics committee (vote of the local ethics committee: 'EK 2067).

2.5 Tissue-engineered vascular graft

To prepare the TEVG, a molding system was created as described previously [21]. The molding system consists of a molding cavity and a cylindrical core. The molding cavity is made of a 6.4 mm inner diameter silicon tube (Carl Roth), and a 3 mm solid steel rod was employed as the core. Both ends of the mold were connected to T-connectors with Luer-lock (Fleima Plastic, Wald-Michelbach, Germany), which were used as sprue and riser. Each sample of the TEVGs are 4 cm long, the inner diameter is 3 mm, and the outer diameter is 6.4 mm. The hydrogel inserted into the mold ($375\text{ }\mu\text{l/cm}$) was a combination of fibrinogen (10 mg/ml) (Thermo Fisher), thrombin (Sigma-Aldrich, Darmstadt, Germany), TBS buffer (Thermo Fisher), CaCl₂ (Sigma-Aldrich) and arterial smooth muscle cells ($10 \times 10^6/\text{ml}$). The polymerization following the molding was confirmed, and the metal core was removed afterward. The lumen was filled with arterial endothelial cells at a concentration of $3 \times 10^6/\text{ml}$. Then the TEVGs were constantly rotated at 1 rpm for 6 h, using a modified peristaltic pump (Ismatec, Wertheim, Germany) to equally distribute the endothelial cells on top of the surface of the lumen. The copolymer TEVGs were prepared separately, and along with the above-described fibrin matrix gel, the VP-co-GMA copolymer solution (40 μl per TEVG) was added. The copolymers were produced via RAFT polymerization as described previously by Peng et al. and Pich et al. [29, 35].

A custom-made close-loop bioreactor system was designed to circulate the medium continuously. A

centrifugal pump (Rs Pro, Plymouth, UK) was attached to transport the media. A pressure sensor (Codan, Lensahn, Germany) and a flow computer (Em-tec GmbH, Finning, Germany) were attached to the bioreactor system. The pressure was maintained from 80 to 120 mmHg, and the flow rate was maintained from 50 to 200 ml/min. Additionally, a clamp (Bürkle GmbH, Bad Bellingen, Germany) was installed to adjust the pressure within the system.

2.6 Synthesis of VP-co-GMA-copolymers via RAFT polymerization

First, the RAFT agent Rhodixan A1 was synthesized as described in the literature [36, 37]. Methyl 2-bromopropionate (Sigma-Aldrich; 40 g, 234 mmol, 1 equiv.) was dissolved in ethanol (300 ml). Potassium ethyl xanthogenate (Sigma-Aldrich; 43.1 g, 268 mmol, 1.1 equiv.) was added stepwise under ice-cooling to the solution within 45 min. Then, the solution was stirred at room temperature for 3 h. The reaction mixture was then filtered and concentrated at 40 °C at a pressure of 175 millibars. Dichloromethane (Sigma-Aldrich; 600 ml) was added, then the organic phase was extracted with demineralized water (4 × 100 ml) before it was dried over magnesium sulfate (Sigma-Aldrich) for 12 h. The solvent was removed under reduced pressure. The RAFT agent was dried under a high vacuum for 8 h.

The copolymers were synthesized via RAFT polymerization as described previously by Peng et al. [29, 35]. The synthesis was performed under an inert atmosphere. For a copolymer with a target molecular weight of approximately 15 000 g/mol and a glycidyl methacrylate (GMA) content of approximately 10 mol%, first, *N*-vinylpyrrolidone (VP, TCI chemicals) and GMA (TCI chemicals) were purified by vacuum distillation to remove the inhibitor. VP (4 g, 36 mmol, 1 equiv.) and the RAFT agent (0.063 g, 0.30 mmol) were dissolved in anisole (Sigma-Aldrich; 6 ml) and degassed with five freeze–pump–thaw–cycles. Then, the reaction temperature was set to 60 °C. A GMA solution (0.51 g, 3.6 mmol, 0.1 equiv.) in anisole (2 ml) and an initiator solution (AIBN, 0.0099 g, 0.060 mmol, 0.002 equiv.) in anisole (0.4 ml) were prepared and degassed with a nitrogen flow under ice-cooling for 30 min. To start the polymerization, the initiator solution was added to the reaction mixture. The GMA solution was added continuously by a syringe pump with a rate of 0.15 ml h^{−1} to the reaction flask. The mixture was cooled down with liquid nitrogen after 24 h to stop the polymerization. The copolymer was precipitated in diethyl ether (400 ml) under ice cooling and dried under vacuum at 40 °C for 36 h.

2.7 Mechanical properties

To measure the burst strength, the TEVGs were cut and opened into rectangular shaped 1 cm² samples and kept inside a custom-made liquid-tight burst chamber. A pressure sensor (Jumu, Munich, Germany), power supply unit and data acquisition I/O device (National Instruments, Austin, TX, USA) were assembled to detect the pressure curve. The sample was kept in between two O-rings in the burst chamber to confirm the proper sealing, and PBS buffer was pumped into the chamber at the rate of 7.5 ml/min via a peristaltic pump (Ismatec) until the sample burst. The pressure courses were recorded via Labview software (National Instruments).

2.7.1 Biaxial strength

To measure the biaxial strength, the TEVGs were cut and sectioned into 1 × 1 cm samples. The samples were clamped from both longitudinal and transversal directions and were pulled from all four sides at a rate of 10 mm/min until the failure point (Zwick Roell, Ulm, Germany). The data were recorded via the test expert software (Zwick Roell). The stress values were calculated by dividing the force by area, and the strain values were calculated by dividing the elongated length by the original length. The young's modulus (Y) values were calculated from the slope of the stress–strain curve. The statistical analysis was performed using one way ANOVA (mean ± SD) with Tukey post hoc corrections.

2.7.2 Suture retention strength

The TEVGs samples were cut diagonally on one side where the suture loop was placed. A size 7.0 suture (Ethicon, USA) was placed 2 mm from the edge according to the DIN EN ISO 7198-A.5.7.4.2.. One side of the TEVG was clamped, and the suture was connected to the uniaxial device (Zwick Roell) and pulled at a rate of 50 mm/min.

2.7.3 Statistical analysis for mechanical tests

For the above-mentioned mechanical tests, all samples (sample size = 6) were analyzed by applying a one-way analysis of variance (ANOVA) with Tukey post hoc correction using Origin Pro software (Northampton, MA, USA).

2.8 Magnetic resonance imaging

A PVDF warp-knitted structure was coated with 0.2% (w/w) SPION-labeled PLGA and then combined with a different number of ¹⁹F-TPU fibers (Lubrizol, Wickliffe, OH,

USA). The textile structures were embedded in 10% gelatin (w/v) and then imaged in a Bruker BioSpec 70/20 USR 7T MRI (Bruker BioSpin GmbH, Rheinstetten, Germany) equipped with a dual-tuned $^1\text{H}/^{19}\text{F}$ transmit/receive volume coil. After obtaining the ^{19}F -NMR spectra of the samples, which showed two distinct peaks at -84.92 and -78.18 ppm, the offset frequency was determined and set at -24.000 Hz.

An ultrashort echo time (UTE) sequence [repetition time: 30 ms; echo time: 0.296 ms; flip angle: 15.0° ; averages: 100; matrix size: 32×32 ; field of view: (40×40) mm²; slice thickness: 5 mm] was used to image the ^{19}F -TPU fibers. In addition, an initial trajectory measurement based on ^1H was performed to reduce distortions caused by the not-so-abundant ^{19}F signal. Qualitative T2-weighted (T2W) images were acquired using a fast spin echo sequence [echo time: 80 ms; repetition time: 4000 ms]. The superimposition and the 3D-rendering of the ^1H and ^{19}F MRI images were obtained using the Imalytics Pre-clinical Software (Gremse-IT GmbH, Aachen, Germany).

2.9 Immunohistochemistry

Based on the protocol described by Koch et al., Carnoy's solution was used to fix the samples [38]. Subsequently, they were washed in ethanol, dehydrated using a dehydration device (Leica TP 1020, Wetzlar, Germany), and embedded in paraffin until further use. Paraffin sections were cut at 5 μm thickness using a microtome (Microm HM 430, Thermofisher Scientific). Before staining, the samples were deparaffinized by serial dilution of xylol and ethanol. Sequenza Staining racks (Thermofisher Scientific) were used to hold in place the samples. 0.1% Triton X-100 aqueous solution containing 5% of normal goat serum (NGS) (Agilent Dako, Santa Clara, CA, USA) was used to block and permeabilize the tissues. Afterward, the primary antibodies were incubated at 37°C for 1 h, and the samples were washed 3 times with PBS for 5 min and then incubated with the respective secondary antibodies for 1 h. After washing the samples 3 times, they were incubated with DAPI (1:500) (Thermofisher Scientific) and mounted with a fluorescent mounting medium (Agilent Dako). The primary antibodies employed for the histological analyses are monoclonal, anti-human α -smooth muscle actin (α -SMA) (Sigma-Aldrich); monoclonal, anti-human CD31 (Sigma-Aldrich); polyclonal, anti-human type I collagen (Acris Antibodies GmbH, Herford, Germany); polyclonal, anti-human type IV collagen (Acris Antibodies GmbH); polyclonal, anti-human elastin (Acris Antibodies GmbH). The secondary antibodies are anti-mouse Alexa Fluor 488, anti-mouse Alexa Fluor 594, and anti-rabbit Alexa Fluor 594 (Thermofisher Scientific). An Axio Imager M2 fluorescence microscope equipped with an AxioCam MRm

Rev.3 camera (Carl-Zeiss, Oberkochen, Germany) with a magnification of $20\times$ was used to acquire the most representative images of each stained section.

2.9.1 Quantitative analysis of immunohistology

All the images used for the quantification of collagen-1, collagen-4, α -SMA, and CD31 were acquired using a fixed exposure time for each channel. Subsequently, the images were post-processed with the AxioVision software (Carl-Zeiss) and quantified via ImageJ (NIH and LOCI, University of Wisconsin) to ensure the same windowing and thresholding.

2.9.2 Statistical analysis

All quantified data of histological samples (sample size = 3) were analyzed by applying one-way analysis of variance (ANOVA) with Tukey post hoc correction using Origin Pro software (Massachusetts, USA).

3 Results

3.1 Electrospinning and molding of the TEVGs

The observation of the orientation and deposition of the fibers was performed by scanning electron microscopy (SEM). The SEM images (Fig. 2A, B) confirm the fiber spreading and the porosity caused by the electrospun coating. There was no evidence of fiber agglomeration or 'beads on string' structure all over the textile scaffold. After molding, the MR imaging confirms a concentric layer of fibrin gel and PLGA + SPION coating on the PVDF mesh (Fig. 2C, D).

3.2 Mechanical strength of the TEVGs

The e-spun coated TEVGs and copolymer TEVGs show significantly higher burst strength than the non-coated TEVGs ($n = 6$) (Fig. 3E). The instantly molded TEVGs (day 0) show lower burst strength whereas, after four days of bioreactor conditioning (day 4), the burst strength shows a notable increase. The highest burst strength achieved was in the copolymer TEVGs at day 4 (617 ± 85 mmHg). The burst strength value of the native artery was found to be (1803 ± 26 mmHg).

All sets of TEVGs ($n = 6$) had higher suture retention strength than the native artery (Fig. 3F). The bioreactor conditioning (day 4 TEVGs) enhanced the suture retention strength, but the electrospun coating does not play an important role in amplifying the suture retention strength as the increase is non-significant. However, the addition of

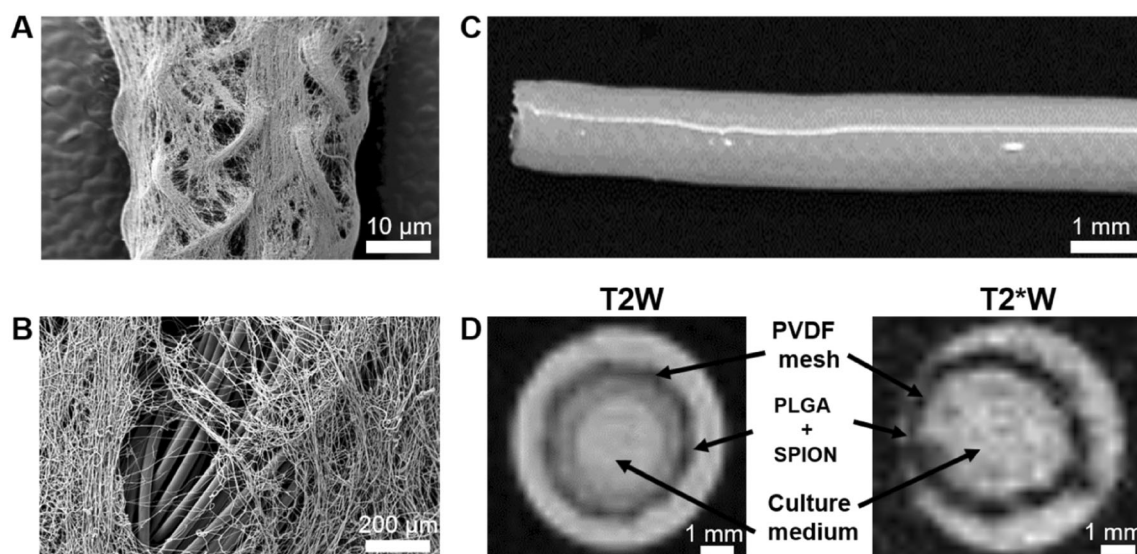


Fig. 2 Electrospun PLGA coated TEVG. **A, B** SEM images of the PLGA and SPION coating on the textile mesh. **C** TEVG after molding. **D** MR images showing the lumen area and the coating upon the textile mesh

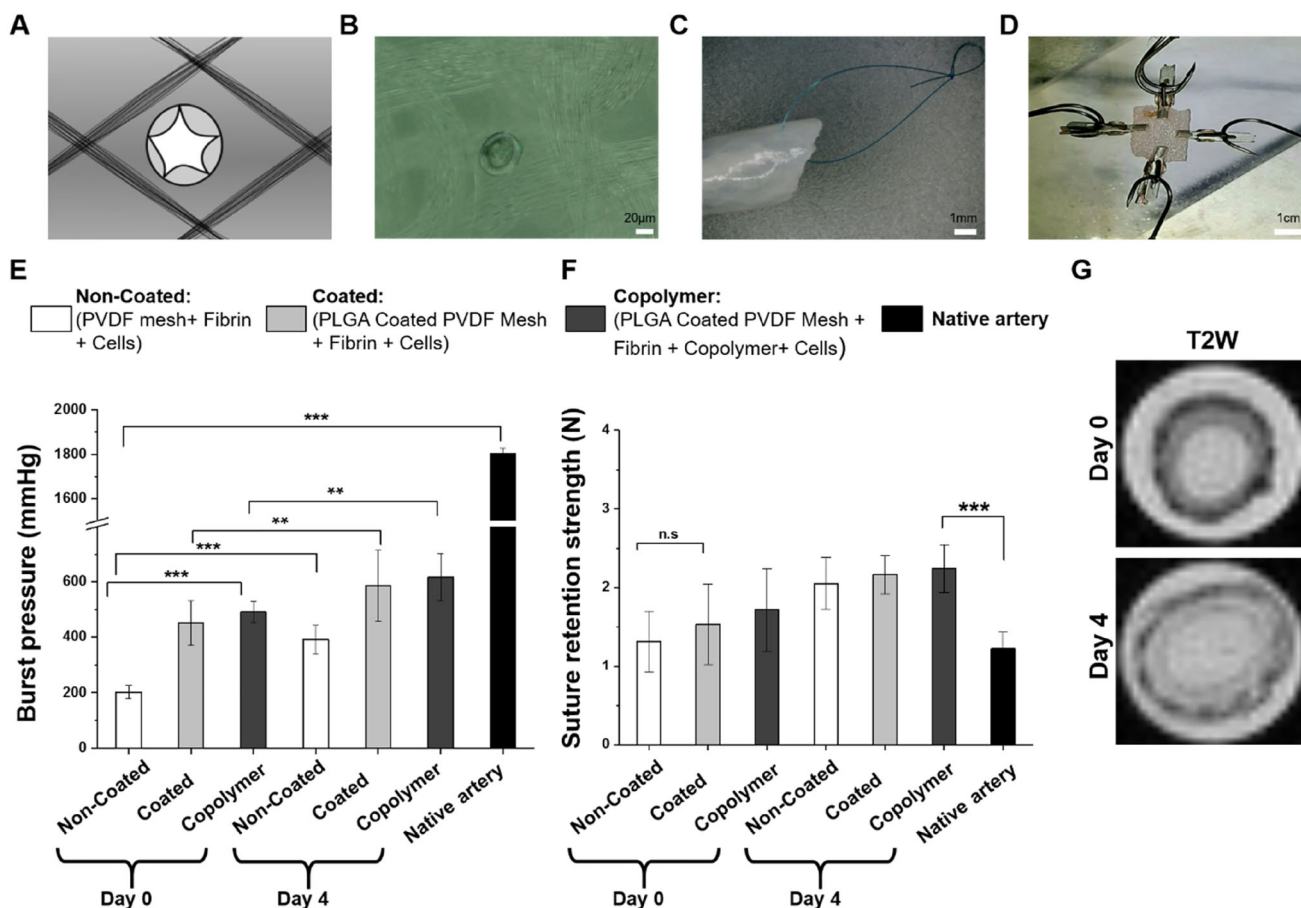


Fig. 3 Mechanical properties of the TEVG. **A** Schematic and representation of hole-like rupture on the TEVG after the burst test between the fibers through the hydrogel. **B** Microscopic image of the ruptured hole between the fibers. **C** The suture loop on a TEVG sample. **D** Biaxial tensile test of a rectangular cut sample. **E** Burst pressure measurement of the TEVGs. **F** Suture retention strength of

TEVGs. **G** Qualitative T2W images of SPION-labeled PLGA coating after 0 and 4 days of bioreactor conditioning. The hypointense signal generated by the SPION decreased over time, correlating with the PLGA coating degradation. Statistical analysis was performed using one way ANOVA (mean \pm SD) with Tukey post hoc corrections (n.s $p > 0.05$, * $p \leq 0.05$, ** $p \leq 0.01$, *** $p \leq 0.001$)

copolymer on the TEVGs increased the burst strength significantly (Fig. 3E). The signal of the SPION-labeled PLGA coating was observed and qualitatively studied via 7T MRI. After 4 days of bioreactor conditioning, the samples ($n = 3$) showed decreased signal intensity in comparison to day 0 (Fig. 3G).

The axial strength of all TEVGs (non-coated, coated, and copolymer) was found to be higher than the radial strength. In comparison to the native artery, the TEVGs at day 0 show a lower strength, whereas the TEVGs at day 4 ($n = 6$) show a higher strength in both the axial and radial measurements. However, the difference is not statistically significant in both cases (Fig. 4A, B). Though the coating and copolymer addition in the TEVGs have no significant impact on enhancing the biaxial tensile strength, it indicates an increasing order. The highest tensile strength was found on the day 4 of copolymer-based TEVGs, where 2.45 ± 0.58 MPa axial strength and 1.50 ± 0.18 MPa radial strength were recorded.

The Young's modulus of the native artery was found to be 1.5 ± 0.81 MPa which was the lowest in comparison to all sets of TEVGs (Fig. 8D). No significant differences were observed between the day 0 coated, non-coated, and copolymer samples. However, the highest young's modulus, 12.31 ± 3.17 MPa, was recorded on the copolymer TEVG at day 4 samples.

3.3 Immunohistochemistry

TEVGs at day 0 showed low expression of collagen type I and type IV and smooth muscle actin. The bioreactor conditioning assisted in expressing the tissue maturation in the TEVGs at day 4. A monolayer of endothelial cells was found in all TEVGs, as evidenced by CD 31 staining. Although the signal of CD31 staining in TEVGs at day 0 was not very intense but TEVGs at day 4 had qualitative progress, and the endothelial layer could be observed clearly (Fig. 5). From the Alpha smooth muscle actin staining, sphere-shaped actin matrices were found near the smooth muscle cells in the freshly molded TEVGs, whereas in the matured TEVGs the geometrical shapes were found to be elliptical or flattened, which were similar to the native artery. Neither the coating nor the copolymer addition has any negative effect on the morphology or growth of the cells (Fig. 6).

The quantitative analysis of immunohistology showed the native artery has the highest area percentage meaning more ECM across all the stainings (Fig. 7A–D). The TEVGs at day 0 have the lowest area percentage, and at day 4 increased area percentage in collagen I, collagen IV, alpha SMA, and CD 31 stainings, but the difference is statistically insignificant.

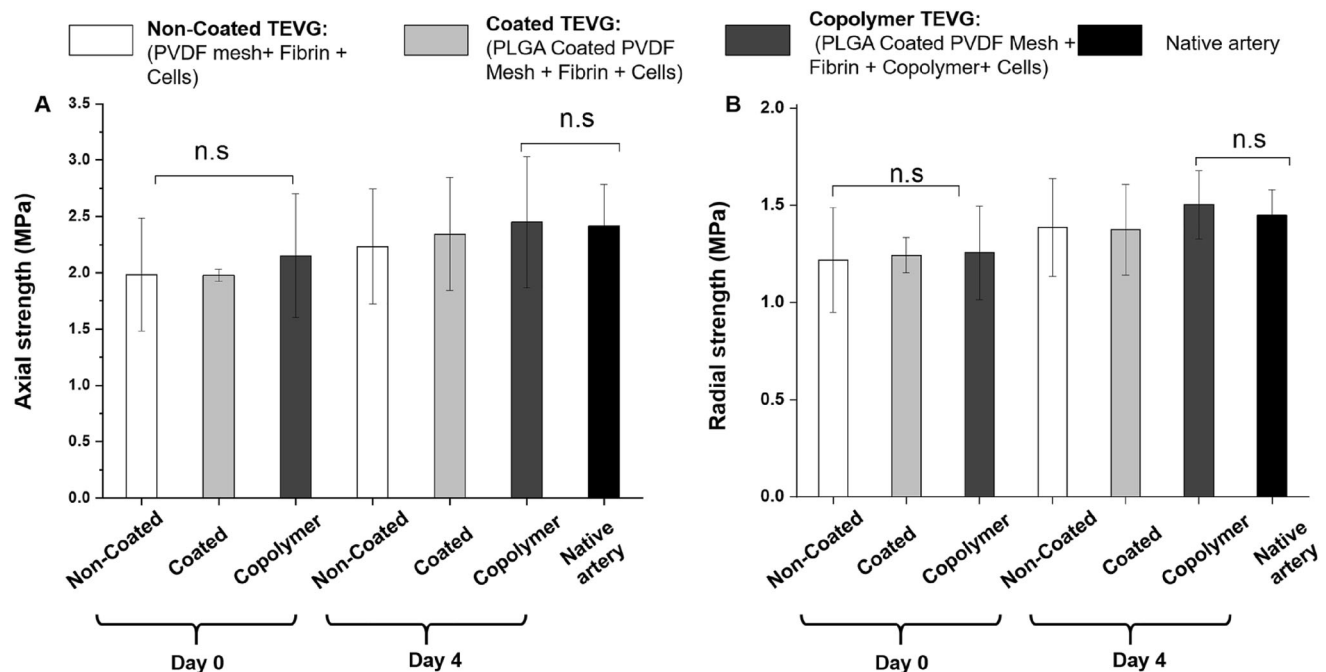


Fig. 4 Biaxial test of the TEVGs. A) Axial strength, B) Radial strength. Statistical analysis was performed using one way ANOVA (mean \pm SD) with Tukey post hoc corrections (n.s $p > 0.05$, * $p \leq 0.05$, ** $p \leq 0.01$, *** $p \leq 0.001$)

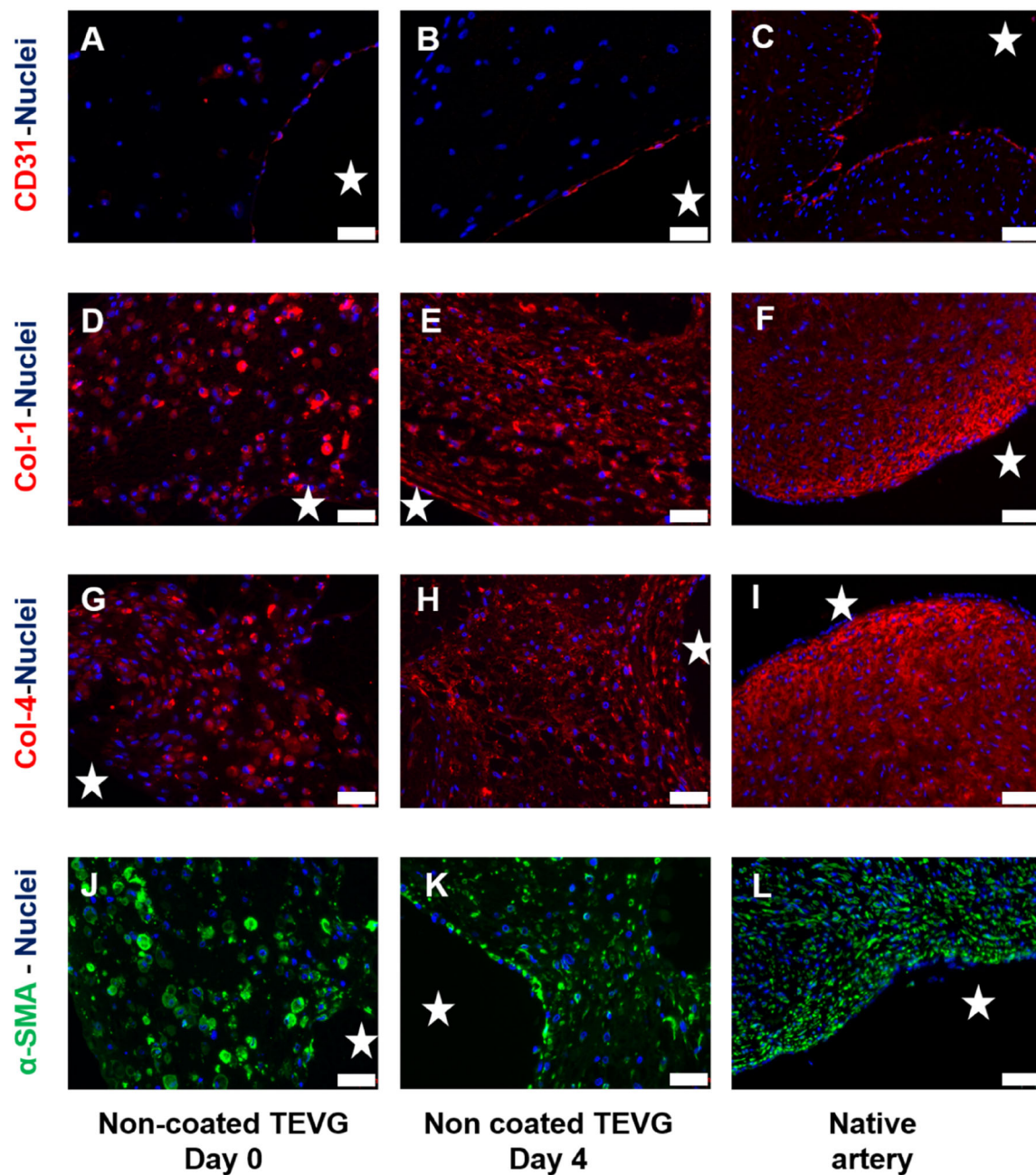


Fig. 5 Immunohistochemical analysis of the non-coated TEVGs in comparison to a native artery (human umbilical cord). **A–C** CD31, DAPI. **D–F** Collagen 1, DAPI. **G–I** Collagen 4, DAPI. **J–L** Alpha SMA, DAPI. Scale bar 20 μm . The stars mark the lumen

3.4 $^1\text{H}/^{19}\text{F}$ Magnetic Resonance Imaging

As illustrated in Fig. 8A, a systematic study was carried out to determine the ideal amount of ^{19}F -TPU fibers needed to generate an adequate signal-to-noise ratio (SNR). Therefore, an increasing number of ^{19}F -TPU fibers was combined with vascular graft textile scaffolds, composed of PVDF warp-knitted structure and 0.2% (w/w) SPION-labeled PLGA. The superimposition of qualitative T2W

and UTE images showed both enhanced visibility of the PLGA layer due to the SPION labeling and increased ^{19}F signal intensity corresponding to a higher number of ^{19}F -TPU fibers (Fig. 8B). Interestingly, both signals are concomitantly detectable and, most importantly, distinguishable without interferences. As additionally shown through the 3D-rendering of the gelatin phantoms, the incorporation of a higher number of ^{19}F -TPU fibers determined a higher SNR, hence a very detailed 3D reconstruction.

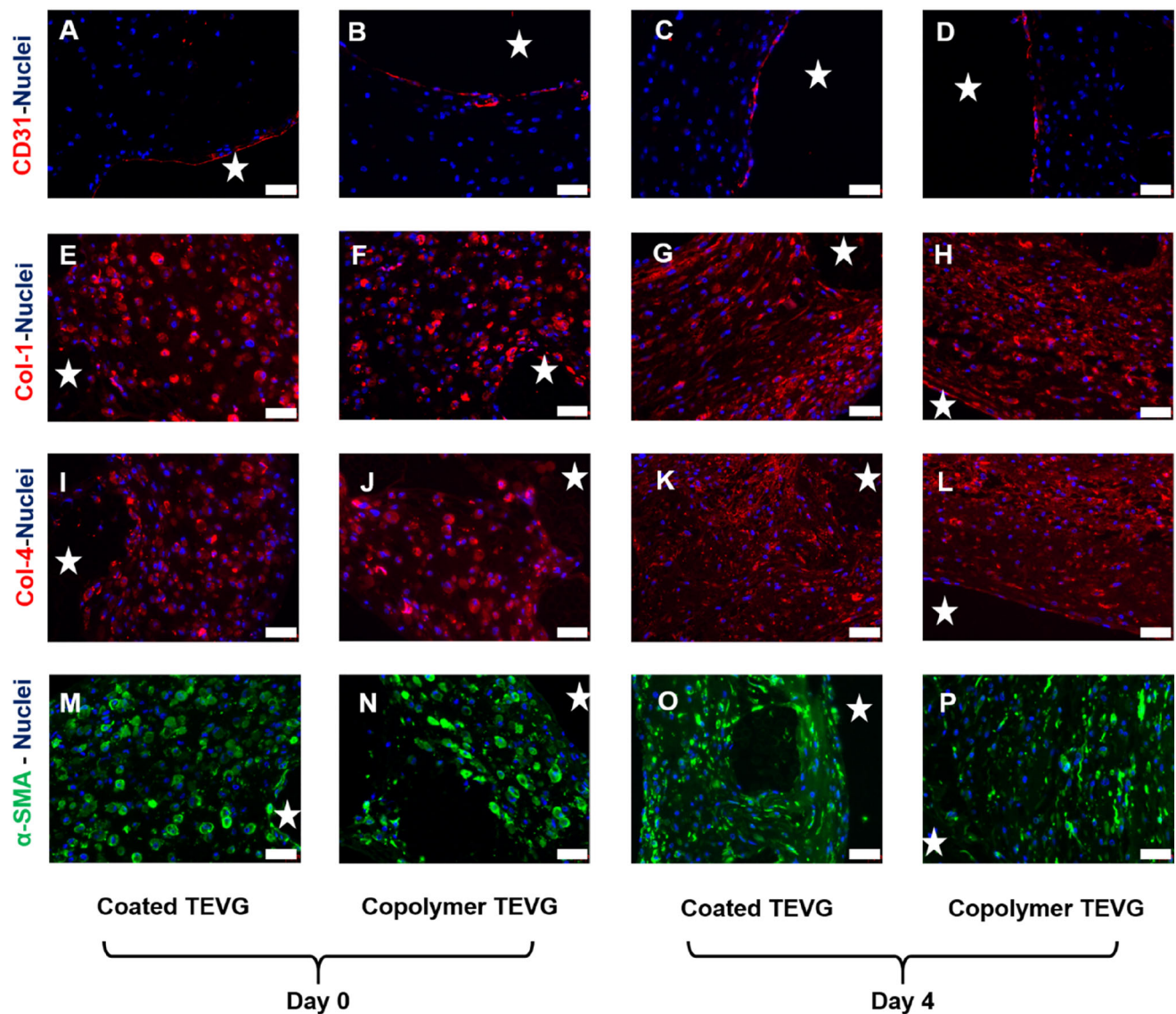


Fig. 6 Immunohistochemical analysis of the coated and copolymer TEVGs. **A–D** CD31, DAPI, **E–H** Collagen 1, DAPI, **I–L** Collagen 4, DAPI, **M–P** Alpha SMA, DAPI. Scale bar 20 μ m. The stars mark the lumen

4 Discussion

In the present study, we describe a further developed concept of our biohybrid textile-reinforced vascular graft to significantly shorten the production time and yet increase the mechanical strength and tissue maturation process. This is an important step toward clinical translation. To achieve this goal, we adopted two strategies which were successfully proved. The first hypothesis was that the initial burst strength could be increased by the application of an additional, electrospun layer of biodegradable PLGA fibers and the second was to integrate VP-co-GMA copolymer to mechanically strengthen the hydrogel as a cell carrier. Both strategies showed two-fold higher burst strength around 451 ± 81 mmHg than the non-coated TEVG

202 ± 24 mmHg when measured just after molding (day 0). After 4 days of bioreactor conditioning, the burst strength of copolymer TEVG was reached 617 ± 85 mmHg (Fig. 3E), and the coated TEVG to 586 ± 125 mmHg. Gui et al. and Syedain et al. have previously reported that the pulsatile flow while conditioning in a bioreactor helps in bringing higher bursts strength [18, 39]. Syedain et al. monitored the burst pressure of their vascular graft over time. After one week of cyclic flow, they burst at a pressure of about 270 mmHg and then increased to 596 ± 28 mmHg and 1366 ± 177 mmHg after 3 and 5 weeks respectively. Yao et al. has found burst pressure of 177 ± 5.3 mmHg on double-layered fibrin based TEVG which was not bioreactor conditioned and these TEVGs could be compared to

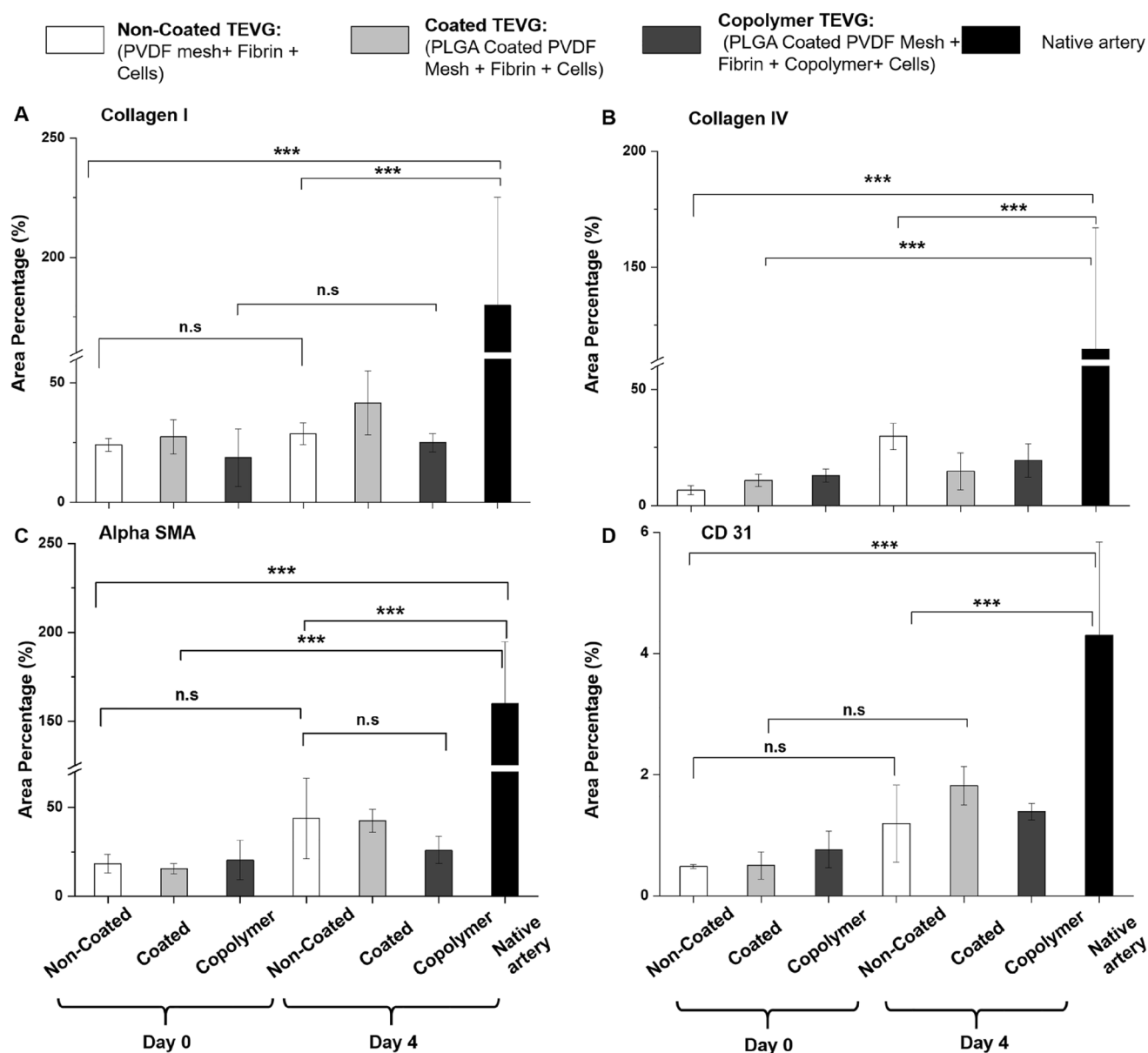


Fig. 7 Quantitative analysis of the histology. **A** Collagen I, **B** collagen IV, **C** Alpha SMA **D** CD31. Statistical analysis was performed using one way ANOVA (mean \pm SD) with Tukey post hoc corrections (n.s $p > 0.05$, * $p \leq 0.05$, ** $p \leq 0.01$, *** $p \leq 0.001$)

the *day 0* TEVGs from our study [40]. Though the textile mesh in our study gives the backbone to support and higher mechanical strength but particularly the burst strength is more affected by the fibrin gel and the electrospun coating. Because the material failure point of a burst test specimen is similar to a pinhole (Fig. 3A, B), which is located in between the knitted fibers, the integration of PLGA coating and copolymer, therefore, increases the burst pressure. The pressure supplied underneath the sample to burst the sample could pass through the gel before it causes any damage to the textile. However, without the textile support, the fibrin gels are not strong enough and could lead to graft failure. Our production technique of biohybrid vascular

graft has a design history, and we have already experimented with the long-term bioreactor conditioning. Having a similar construct, B. Tschoeke et al. has found 263 mmHg of burst pressure and 460 mmHg of burst pressure after 14 days and 21 days of bioreactor conditioning, respectively [22, 23]. Wolf et al. have found 872 mmHg of burst pressure after 14 days of bioreactor conditioning by further modifying the bioreactor [24]. The burst strength increases when the TEVG is kept for a longer time. However, the main goal here is to initially enhance the burst strength before the complete ECM maturation by modifying the hydrogel with a copolymer and adding the extra electrospun layer. Doing more

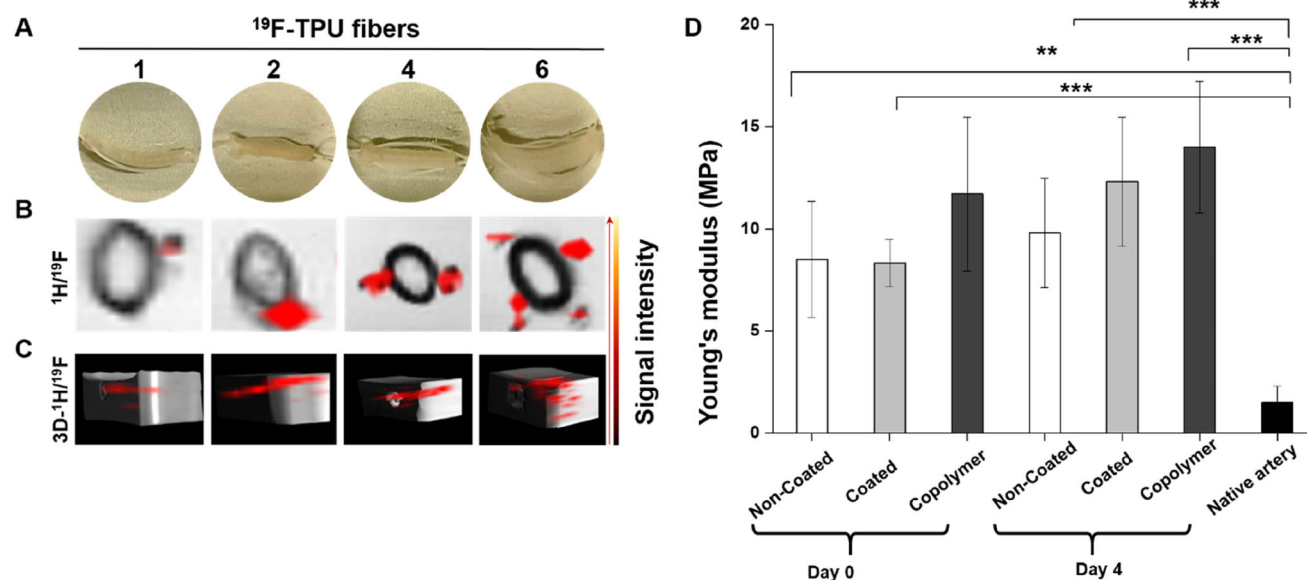


Fig. 8 ^{19}F -TPU visibility via MRI. **A** Gelatin phantoms containing 0.2% (w/w) of SPION-labeled PLGA electrospun onto a PVDF warp-knitted scaffold combined with a different number of ^{19}F -TPU fibers. **B** Transversal planes of superimposed grayscale T2W and “hot spot” UTE images show the increased ^{19}F signal intensity correlating to a

higher number of ^{19}F -TPU fibers. **C** 3D rendering of superimposed $^1\text{H}/^{19}\text{F}$ -MR images of the samples. **D** Young's modulus of the TEVGs and native artery. Statistical analysis was performed using one way ANOVA (mean \pm SD) with Tukey post hoc corrections (n.s $p > 0.05$, * $p \leq 0.05$, ** $p \leq 0.01$, *** $p \leq 0.001$)

prolonged cultivation will shift our focus to achieving higher and higher native-like burst strength, which is not the immediate requirement in the clinic. The burst strength we gained (617 ± 85 mmHg) only in 4 days is six-fold higher than the systolic arterial pressure. The highest reported blood pressure on any human is 370 mmHg [41]. Our next focus will aim towards further reducing the bioreactor conditioning time and achieving peri-operative implantation. The perioperative tissue engineering method could become potentially the most vital approach to serve acute vascular dysfunction.

The suture retention strength of TEVGs was even higher than native artery because of the integrated textile reinforcement (Fig. 3F). The warp knitted textile mesh has a loop-like structure, which helps in retaining the suture for a longer time before failure. The bioreactor conditioning further positively influenced the suture retention strength as higher values were recorded on day 4 TEVG. The textile scaffold being the major factor here, its influence mainly determines the strength. Still, the combination of PLGA coating and copolymer in the TEVGs also has a slight impact, enhancing the suture retention strength. To obtain precise data for future clinical study, a 7.0 ProleneTM suture was used [42, 43]. Despite using small diameter sutures our vascular grafts have shown much higher suture retention strength than synthetic polymer-based vascular grafts [13, 44]. Even very high suture retention strength like 6.3 ± 2.8 N and 4.5 ± 1 N have been achieved by Tschoeke et al. and Dimopoulos et al., respectively, in

different kinds of TEVGs [23, 45]. However, in these experiments, 4.0 prolene suture ware was used, whereas in vascular surgeries the use of 4.0 suture size has rarely been found in literature and the size is too big to be employed in small diameter vascular surgery. According to the DIN EN ISO 7198, the suture size must be close to clinical relevance to measuring the suture retention strength, hence a 7.0 size suture was used.

Though the tensile strength of vascular grafts has been widely studied by other researchers, biaxial studies are not found [46–48]. Some biaxial studies are done one after another axis but not pulled from both sides at the same time [49]. The axial strength of the TEVGs was higher than the radial strength because of the textile structure. The rhombus-like structure of the wrap knitting makes the axial pulling angle lesser than the radial, therefore resulting in higher tensile strength. The fibrin gel and the maturation have a lesser effect on the biaxial test because most of the strength develops from the textile mesh, unlike the burst strength study. However, when compared to the native artery, our TEVGs have similar tensile strength in both axial and radial directions. Young's modulus was also significantly higher in TEVGs than in the native artery (1.5 ± 0.81 MPa). The nondegradable PVDF textile contributes more to the strength of the TEVGs, resulting in higher elastic modulus. Inoue et al. have recently discussed about the comparison of TEVGs with different native arteries. They tested and found 5.41 ± 1.16 MPa of Young's modulus in raw TEVGs and after crosslinking by

glutaraldehyde, they found 7.65 ± 1.18 MPa. Along with TEVGs, they have compared the young's modulus of native veins and arteries and found 1.5 MPa and 3 MPa, respectively [50].

The production method of tissue-engineered grafts, the bioreactor, and the conditioning strategy plays a vital role in maintaining and growing the extracellular matrices [30, 51–53]. The immunohistological analysis has proved the development of essential extracellular matrices in just 4 days of bioreactor conditioning, thus, the molding technique and bioreactor used in the present study have a supportive and positive impact. The electrospun layer and copolymer have no negative impact on the ECM development, and on the other hand, they also do not show a further positive impact on ECM maturation, summarizing a neutral effect. Previous studies have shown that in the phase of tissue remodeling, the collagen amount could increase, decrease or remain the same depending on their enzyme activities [24, 52, 53]. In the present study, the collagen has shown a very good maturation in the TEVGs at day 4 than the TEVGs at day 0. The quantitative analysis of immunohistology shows a significant difference between native arteries and all sets of TEVGs across all the stainings. Achieving a similar ECM to the native artery in just 4 days was neither our hypothesis nor expected. Substantially shortening production time and yet having sufficient mechanical strength with increasing ECM was our expectation and the results obtained met our hypothesis.

In regards to the imaging approach, TEVG's scaffold traceability was demonstrated by MRI. The PLGA degradation was monitored over 4 days and qualitatively analysed. The signal intensity was found to be weaker after 4 days of bioreactor conditioning, indirectly indicating the degradation of the PLGA coating. The monitoring of the degradation of this biocompatible TEVG component could be used as an indirect marker to predict patient compliance and ameliorate their outcomes [54, 55]. Subramanian et al. and Prabhakaran et al. had also previously discussed about the PLGA degradation in relation to tissue response [55, 56]. However, these studies were carried out via invasive imaging methods, thus after animal sacrifice or termination of the experiment. On the other hand, as shown in our previous publication, we recently proposed a novel imaging approach that showed the replacement of the degradable PLGA layer with new ECM deposition and the monitoring of the onset of inflammatory reaction in a non-invasive and non-destructive way [33]. Indeed, the longitudinal monitorability of the SPION-labeled PLGA textile component degradation was proved both *in vitro* and *in vivo* without harming or sacrificing the animals until the end of the experiment. Moreover, the ECM production and TEVG's endothelial functionality were also investigated via non-invasive and non-destructive molecular MRI and

targeted ultrasound. In addition, also here in our study, we showed the successful employment of this novel imaging approach to qualitatively assess the SPION-labeled PLGA layer degradation while TEVGs were still under bioreactor conditioning.

On the other hand, we were able to develop a novel textile scaffold by combining ^{19}F -TPU and SPION-labeled PLGA, proving the visibility and detectability of both SPION-labeled PLGA and ^{19}F -TPU fibers via $^1\text{H}/^{19}\text{F}$ MRI. During the last decades, several new strategies and approaches have been proposed to modify MRI scanners, customize coils and software, and develop fluorinated polymeric nanoparticles [57, 58] or metallic nanoparticles [59], micelles [60], nanoemulsions [61], or mesoporous silica spheres [62] as *in vivo* cell tracking and trafficking system [63] or to be integrated into tissue-engineered constructs [34, 64]. Therefore, the employment of non-invasive multimodal imaging modalities, as such we demonstrated herein to monitor the structure of our TEVGs, might provide tremendous advantages in several theranostic and therapeutic applications.

In conclusion, we here present a biohybrid tissue-engineered vascular graft with a distinct shortage of production time yet possessing sufficient mechanical strength. We were able to prove that the initial burst strength of the TEVGs can be enhanced by coating a layer of electrospun PLGA onto a PVDF textile mesh and integrating a VP-co-GMA copolymer into a fibrin cell carrier hydrogel. Applying this strategy allows to reduce the bioreactor conditioning time to 4 days instead of several weeks as just in 4 days of conditioning, sufficient ECM maturation can also be achieved.

Herein, we confirmed once again the increased visibility of our TEVGs after SPION-labeling and non-invasive qualitative assessment via 7T MRI. In addition, we demonstrated the employment of a novel imaging approach, which allowed the coupled visualization of SPION-labeled and ^{19}F -TPU fibers via $^1\text{H}/^{19}\text{F}$ -MRI without interferences and overlapping of the signals.

In conclusion, the several strategies proposed throughout this study to effectively shorten TEVGs bioreactor conditioning time without jeopardizing their mechanical strength and to develop novel non-invasive and non-destructive multimodal imaging approaches to increase the visibility and monitorability of our vascular prostheses might strongly foster the *in vivo* applicability of our model of biohybrid tissue-engineered vascular grafts.

Supplementary Information The online version contains supplementary material available at <https://doi.org/10.1007/s13770-022-00482-0>.

Acknowledgements This work was supported by the German Research Foundation in the Package Proposals PAK 961 (DFG –

31. Xiao YD, Paudel R, Liu J, Ma C, Zhang ZS, Zhou SK. MRI contrast agents: classification and application (review). *Int J Mol Med*. 2016;38:1319–26.
32. Mertens ME, Hermann A, Bühren A, Olde-Damink L, Möckel D, Gremse F, et al. Iron oxide-labeled collagen scaffolds for non-invasive MR imaging in tissue engineering. *Adv Funct Mater*. 2014;24:754–62.
33. Rama E, Mohapatra SR, Melcher C, Nolte T, Dadfar SM, Brueck R, et al. Monitoring the remodeling of biohybrid tissue-engineered vascular grafts by multimodal molecular imaging. *Adv Sci (Weinh)*. 2022;9:e2105783.
34. Lammers T, Mertens ME, Schuster P, Rahimi K, Shi Y, Schulz V, et al. Fluorinated polyurethane scaffolds for (19)F magnetic resonance imaging. *Chem Mater*. 2017;29:2669–71.
35. Peng H, Rübsam K, Hu C, Jakob F, Schwaneberg U, Pich A. Stimuli-responsive poly(N-vinyl lactams) with glycidyl side groups: synthesis, characterization, and conjugation with enzymes. *Biomacromolecules*. 2019;20:992–1006.
36. Van Nieuwenhove I, Maji S, Dash M, Van Vlierberghe S, Hoogenboom R, Dubrue P. RAFT/MADIX polymerization of N-vinylcaprolactam in water–ethanol solvent mixtures. *Polym Chem*. 2017;8:2433–7.
37. Beija M, Marty JD, Destarac M. Thermoresponsive poly(N-vinyl caprolactam)-coated gold nanoparticles: sharp reversible response and easy tunability. *Chem Commun (Camb)*. 2011;47:2826–8.
38. Koch S, Stappenbeck N, Cornelissen CG, Flanagan TC, Mela P, Sachweh J, et al. Tissue engineering: selecting the optimal fixative for immunohistochemistry. *Tissue Eng Part C Methods*. 2012;18:976–83.
39. Syedain ZH, Meier LA, Bjork JW, Lee A, Tranquillo RT. Implantable arterial grafts from human fibroblasts and fibrin using a multi-graft pulsed flow-stretch bioreactor with noninvasive strength monitoring. *Biomaterials*. 2011;32:714–22.
40. Yao L, Liu J, Andreadis ST. Composite fibrin scaffolds increase mechanical strength and preserve contractility of tissue engineered blood vessels. *Pharm Res*. 2008;25:1212–21.
41. Narloch JA, Brandstater ME. Influence of breathing technique on arterial blood pressure during heavy weight lifting. *Arch Phys Med Rehabil*. 1995;76:457–62.
42. Haller JR. Basic techniques in microvascular anastomosis. *Facial Plast Surg*. 1996;12:3–7.
43. Meng X, Wang X, Jiang Y, Zhang B, Li K, Li Q. Suture retention strength of P(LLA-CL) tissue-engineered vascular grafts. *RSC Adv*. 2019;9:21258–64.
44. Hoerstrup SP, Zünd G, Sodian R, Schnell AM, Grünenfelder J, Turina MI. Tissue engineering of small caliber vascular grafts☆. *Eur J Cardiothorac Surg*. 2001;20:164–9.
45. Dimopoulos A, Markatos DN, Mitropoulou A, Panagiotopoulos I, Koletsis E, Mavrilas D. A novel polymeric fibrous microstructured biodegradable small-caliber tubular scaffold for cardiovascular tissue engineering. *J Mater Sci Mater Med*. 2021;32:21.
46. Henry JJD, Yu J, Wang A, Lee R, Fang J, Li S. Engineering the mechanical and biological properties of nanofibrous vascular grafts for in situ vascular tissue engineering. *Biofabrication*. 2017;9:035007.
47. Stoiber M, Grasl C, Moscato F, Schima H. Mechanical testing of vascular grafts. In: Walpoth BH, Bergmeister H, Bowlin GL, Kong D, Rotmans JI, Zilla P, editors. *Tissue-engineered vascular grafts*. Cham: Springer; 2020. p. 35–61.
48. Mun CH, Jung Y, Kim SH, Lee SH, Kim HC, Kwon IK, et al. Three-dimensional electrospun poly(lactide-co-ε-caprolactone) for small-diameter vascular grafts. *Tissue Eng Part A*. 2012;18:1608–16.
49. Mauri A, Zeisberger SM, Hoerstrup SP, Mazza E. Analysis of the uniaxial and multiaxial mechanical response of a tissue-engineered vascular graft. *Tissue Eng Part A*. 2013;19:583–92.
50. Inoue T, Kanda K, Yamanami M, Kami D, Gojo S, Yaku H. Modifications of the mechanical properties of in vivo tissue-engineered vascular grafts by chemical treatments for a short duration. *PLoS One*. 2021;16:e0248346.
51. Stacy MR, Naito Y, Maxfield MW, Kurobe H, Tara S, Chan C, et al. Targeted imaging of matrix metalloproteinase activity in the evaluation of remodeling tissue-engineered vascular grafts implanted in a growing lamb model. *J Thorac Cardiovasc Surg*. 2014;148:2227–33.
52. Naito Y, Williams-Fritze M, Duncan DR, Church SN, Hibino N, Madri JA, et al. Characterization of the natural history of extracellular matrix production in tissue-engineered vascular grafts during neovessel formation. *Cells Tissues Organs*. 2012;195:60–72.
53. Cummings I, George S, Kelm J, Schmidt D, Emmert MY, Weber B, et al. Tissue-engineered vascular graft remodeling in a growing lamb model: expression of matrix metalloproteinases. *Eur J Cardio-thorac Surg*. 2012;41:167–72.
54. Keidar Z, Pirmisashvili N, Leiderman M, Nitecki S, Israel O. 18F-FDG uptake in noninfected prosthetic vascular grafts: incidence, patterns, and changes over time. *J Nucl Med*. 2014;55:392–5.
55. Prabhakaran MP, Kai D, Ghasemi-Mobarakeh L, Ramakrishna S. Electrospun biocomposite nanofibrous patch for cardiac tissue engineering. *Biomed Mater*. 2011;6:055001.
56. Subramanian A, Krishnan UM, Sethuraman S. In vivo biocompatibility of PLGA-polyhexylthiophene nanofiber scaffolds in a rat model. *Biomed Res Int*. 2013;2013:39051.
57. Srinivas M, Morel PA, Ernst LA, Laidlaw DH, Ahrens ET. Fluorine-19 MRI for visualization and quantification of cell migration in a diabetes model. *Magn Reson Med*. 2007;58:725–34.
58. Srinivas M, Turner MS, Janjic JM, Morel PA, Laidlaw DH, Ahrens ET. In vivo cytometry of antigen-specific t cells using 19F MRI. *Magn Reson Med*. 2009;62:747–53.
59. Gentilini C, Evangelista F, Rudolf P, Franchi P, Lucarini M, Pasquato L. Water-soluble gold nanoparticles protected by fluorinated amphiphilic thiolates. *J Am Chem Soc*. 2008;130:15678–82.
60. Hill LK, Frezzo JA, Katyal P, Hoang DM, Ben Youss Gironde Z, Xu C, et al. Protein-engineered nanoscale micelles for dynamic (19)F magnetic resonance and therapeutic drug delivery (in Eng). *ACS Nano*. 2019;13:2969–85.
61. Neubauer AM, Myerson J, Caruthers SD, Hockett FD, Winter PM, Chen J, et al. Gadolinium-modulated 19F signals from perfluorocarbon nanoparticles as a new strategy for molecular imaging. *Magn Reson Med*. 2008;60:1066–72.
62. Vernikouskaya I, Pochert A, Lindén M, Rasche V. Quantitative (19)F MRI of perfluoro-15-crown-5-ether using uniformity correction of the spin excitation and signal reception. *MAGMA*. 2019;32:25–36.
63. Srinivas M, Heerschap A, Ahrens ET, Figdor CG, de Vries IJ. (19)F MRI for quantitative in vivo cell tracking. *Trends Biotechnol*. 2010;28:363–70.
64. Constantinides C, Basnett P, Lukasiewicz B, Carnicer R, Swider E, Majid QA, et al. In vivo tracking and 1H/19F magnetic resonance imaging of biodegradable polyhydroxyalkanoate/poly-caprolactone blend scaffolds seeded with labeled cardiac stem cells. *ACS Appl Mater Interfaces*. 2018;10:25056–68.

Springer Nature or its licensor holds exclusive rights to this article under a publishing agreement with the author(s) or other rightsholder(s); author self-archiving of the accepted manuscript version of

this article is solely governed by the terms of such publishing agreement and applicable law.

Supplementary information:

Table S1: p values obtained from the statistical analysis. Column 1 indicates the combinations, and the other columns (2-5) show the P value data for the performed tests.

combinations	P values			
	Burst strength test	Suture retention strength	axial strength	radial strength
Coated TEVG day 0 , Not Coated TEVG day 0	1,36732	0.9479	1,00	0.99999
CO-Polymer TEVG day 0, Not Coated TEVG day 0	0,0790723	0.51739	0.99587	0.99992
CO-Polymer TEVG day 0 , Coated TEVG day 0	0.95667	0.97741	0.99495	1
Not Coated TEVG day 4 , Not Coated TEVG day 0	98,6148	0.0255	0.96804	0.80529
Not Coated TEVG day 4, Coated TEVG day 0	0.77632	0.23255	0.9639	0.89998
Not Coated TEVG day 4 , CO-Polymer TEVG day 0	0.22348	0.71922	0.99993	0.93063
Coated TEVG day 4, Not Coated TEVG day 0	0,00194105	0.00636	0.83686	0.84742
Coated TEVG day 4 , Coated TEVG day 0	0.03517	0.08015	0.82564	0.9283
Coated TEVG day 4 , CO-Polymer TEVG day 0	0.27243	0.39229	0.99128	0.95269
Coated TEVG day 4, Not Coated TEVG day 4	69,3623	0.99821	0.99958	1
CO-Polymer TEVG day 4, Not Coated TEVG day 0	0,00112218	0.00244	0.6135	0.24159
CO-Polymer TEVG day 4 , Coated TEVG day 0	0.00483	0.03586	0.59867	0.34481
CO-Polymer TEVG day 4 , CO-Polymer TEVG day 0	0.05848	0.22314	0.92517	0.39716
CO-Polymer TEVG day 4, Not Coated TEVG day 4	0,73362	0.97421	0.9836	0.95434
CO-Polymer TEVG day 4 , Coated TEVG day 4	0.9874	0.99985	0.99969	0.93276
Native artery , Not Coated TEVG day 0	0	0.99964	0.68647	0.48046
Native artery, Coated TEVG day 0	0	0.79278	0.67211	0.61618
Native artery , CO-Polymer TEVG day 0	0	0.29106	0.95524	0.67546
Native artery , Not Coated TEVG day 4	0	0.00905	0.99281	0.99809
Native artery , Coated TEVG day 4	0	0.00209	0.99996	0.99564
Native artery , CO-Polymer TEVG day 4	0	77,61	1,00	0.9993

Top view of a TEVG:

Figure S 1

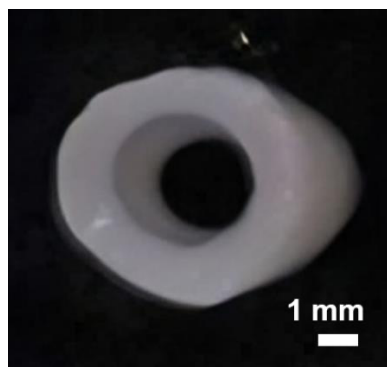


Figure S1:: Top view of a TEVG after molding



Novel Bioreactor Design for Non-invasive Longitudinal Monitoring of Tissue-Engineered Heart Valves in 7T MRI and Ultrasound

Saurav Ranjan Mohapatra¹ · Elena Rama² · Maximillian P. Werner¹ · Tobias Call¹ · Tanja Loewenberg¹ · Alexander Loewen¹ · Christian Apel¹ · Fabian Kiessling² · Stefan Jockenhoevel¹

Received: 29 May 2024 / Accepted: 2 October 2024 / Published online: 22 October 2024
© The Author(s) 2024

Abstract

The development of cardiovascular implants is abundant, yet their clinical adoption remains a significant challenge in the treatment of valvular diseases. Tissue-engineered heart valves (TEHV) have emerged as a promising solution due to their remodeling capabilities, which have been extensively studied in recent years. However, ensuring reproducible production and clinical translation of TEHV requires robust longitudinal monitoring methods.

Cardiovascular magnetic resonance imaging (MRI) is a non-invasive, radiation-free technique providing detailed valvular imaging and functional assessment. To facilitate this, we designed a state-of-the-art metal-free bioreactor enabling dynamic MRI and ultrasound imaging. Our compact bioreactor, tailored to fit a 72 mm bore 7 T MRI coil, features an integrated backflow design ensuring MRI compatibility. A pneumatic drive system operates the bioreactor, minimizing potential MRI interference. The bioreactor was digitally designed and constructed using polymethyl methacrylate, utilizing only polyether ether ketone screws for secure fastening. Our biohybrid TEHV incorporates a non-degradable polyethylene terephthalate textile scaffold with fibrin matrix hydrogel and human arterial smooth muscle cells.

As a result, the bioreactor was successfully proven to be MRI compatible, with no blooming artifacts detected. The dynamic movement of the TEHVs was observed using gated MRI motion artifact compensation and ultrasound imaging techniques. In addition, the conditioning of TEHVs in the bioreactor enhanced ECM production. Immunohistology demonstrated abundant collagen, α -smooth muscle actin, and a monolayer of endothelial cells throughout the valve cusp. Our innovative methodology provides a physiologically relevant environment for TEHV conditioning and development, enabling accurate monitoring and assessment of functionality, thus accelerating clinical acceptance.

Keywords Tissue engineering · Bioreactor · Cardiovascular implants · Non-invasive imaging · 7T MRI

Introduction

The unmet clinical needs caused by cardiovascular diseases such as endocarditis and calcification have led to a substantial increase in heart valve replacements worldwide. Traditional prosthetic heart valves, though effective, have notable limitations, including thrombosis risk, structural deterioration, and lack of growth potential in younger patients. Mechanical valves, while durable, require lifelong anticoagulation, which raises the risk of bleeding. Alternatively, bioprosthetic valves are susceptible to structural deterioration, especially in younger patients, often leading to the need for reoperation [1, 2]. Consequently, cardiovascular tissue engineering has emerged as a promising solution to address these challenges, aiming to replicate the structure, function, and dynamics of native heart valves while

Associate Editor Umberto Morbiducci oversaw the review of this article.

✉ Stefan Jockenhoevel
jockenhoevel@ame.rwth-aachen.de

¹ Department of Biohybrid & Medical Textile (BioTex), Center for Biohybrid Medical Systems (CBMS), Institute for Applied Medical Engineering, RWTH Aachen University, Forckenbeckstr. 55, 52074 Aachen, Germany

² Institute for Experimental Molecular Imaging, RWTH Aachen University, Forckenbeckstr. 55, 52074 Aachen, Germany

promoting long-term integration and functionality within the body [3–6]. However, integrating tissue-engineered valves into the recipient's body is highly complex. It poses crucial challenges, such as the degradation of synthetic scaffolds and the remodeling and maturation of the engineered tissue. For this reason, the translation of the various existing concepts into clinical applications has not yet taken place. To assess the safety and performance of a newly developed implant, it is important to monitor the entire life cycle. This starts with the *in vitro* conditioning phase to observe quality parameters to define release criteria and ends with clinical follow-up examinations of the implant in the patient.

In recent decades, cardiovascular MRI and ultrasound have emerged as non-invasive, radiation-free alternatives for valvular heart conditions, providing detailed valve images and precise stenosis/regurgitation assessment [7]. While non-invasive tests like ECG and auscultation remain effective, their outcomes hinge on both physician and patient [8].

With the objective of advancing biohybrid tissue-engineered implants for clinical application, our research group demonstrated the MR imaging of tissue-engineered vascular grafts both *in vitro* and *in vivo* [9]. Subsequently, we presented the imaging concept of monitoring the deposition of extracellular matrix (ECM) components and the onset of potential inflammatory reactions in vascular grafts in 7 T MRI and ultrasound imaging modalities [10, 11].

MRI offers distinct advantages over other imaging modalities like CT and X-rays for *in vitro* heart valve imaging. It provides excellent soft-tissue contrast and greater penetration depth, allowing for highly detailed and accurate assessments of heart valve structures. In addition, MRI does not involve ionizing radiation, which is beneficial for potential human applications. However, it is important to note that CT technology is continuously evolving, with improvements in resolution and imaging speed making it an increasingly competitive option, despite its reliance on radiation [12–14]. Recognizing the increasing demand for comprehensive valve replacement solutions, we have extended these imaging techniques to the evaluation of heart valves. However, imaging of heart valves presents distinct challenges compared to vascular grafts due to their intricate structure and dynamic movement.

Several attempts have been made to create bioreactors for conditioning heart valves [15–20], where designs were adapted primarily for the movement of the valves and providing a suitable environment for overall cell growth.

Karim et al. developed a tissue reactor for decellularizing porcine heart valves and then recellularizing them with human vascular cells, optimizing conditions to withstand cyclic pulmonary pressures [21]. Tefft et al. engineered a bioengineered heart valve and bioreactor that maintained cell viability for up to 2 weeks, focusing on sustaining pressure and flow conditions [22]. Similarly, Syedain et al.

created fibrin-based heart valves and bioreactors, emphasizing their ability to endure cyclic pulmonary pressures [23]. However, none of these studies incorporated non-invasive imaging techniques like MRI. In contrast, our bioreactor integrates MRI capabilities, providing a significant advantage by enabling detailed, non-invasive monitoring of valve function and tissue growth, thus enhancing the overall evaluation and management of the bioreactor system.

Voss et al. (2022) have recently made remarkable functional bioreactors, but they were equipped with an actuator motor to open and close the valve, which does not qualify for MRI modality [24]. Even though there are previous approaches that used pneumatic drives [25, 26], they also did not have any non-invasive imaging possibility.

Non-invasive imaging like MRI offers the ability to acquire multiple types of imaging contrasts, and dynamic MRI enables real-time monitoring of physiological processes. 7 Tesla (7 T) MRI has emerged as a potential tool for cardiovascular imaging due to its ability to provide higher spatial resolution and tissue contrast than 3 T MRI [27], allowing for clear visualization of complex structures [28].

Therefore, our focus was on conducting tests using lab-sized and small animal-sized MRI devices (with a bore diameter of 70 to 75 mm). This approach allows for the exploration of small tissue-engineered heart valves, which is particularly relevant for studying young patients. The 7 T MRI offers clear advantages over lower field strengths like 3 T or 1.5 T, including superior resolution, higher signal-to-noise ratio (SNR), and enhanced soft-tissue contrast. These benefits enable much finer visualization of lesions, more precise detection of small anatomical details, and better assessment of subtle movements, which are crucial for detailed imaging studies. In the design of a small-bore bioreactor, we implemented an integrated backflow design, facilitating circulation from the ventricle to the aorta within a single cylindrical structure. The bioreactor comprises three essential chambers: the observation chamber for examining the valves, the fixation chamber for securing the valves, and the air chamber for compressing air.

The TEHVs were fabricated by combining medical-grade polyethylene terephthalate (PET) textile and fibrin matrix gel along with human arterial smooth muscle cells and were sutured on a silicon conduit (Fig 1a–b) as previously described [24, 29]. To improve the detectability of the TEHVs in MRI, the PET scaffold was coated with superparamagnetic iron oxide nanoparticles (SPION)-labeled poly(lactic glycolic acid) (PLGA) electrospun fibers.

In this study, we present a novel bioreactor design for the conditioning of aortic tissue-engineered heart valves (TEHV) that supports multi-modal imaging (Fig 1 c–e). We demonstrate the MRI compatibility of our bioreactor without encountering blooming artifacts, allowing for clear observation of the dynamic movement of TEHVs using gated

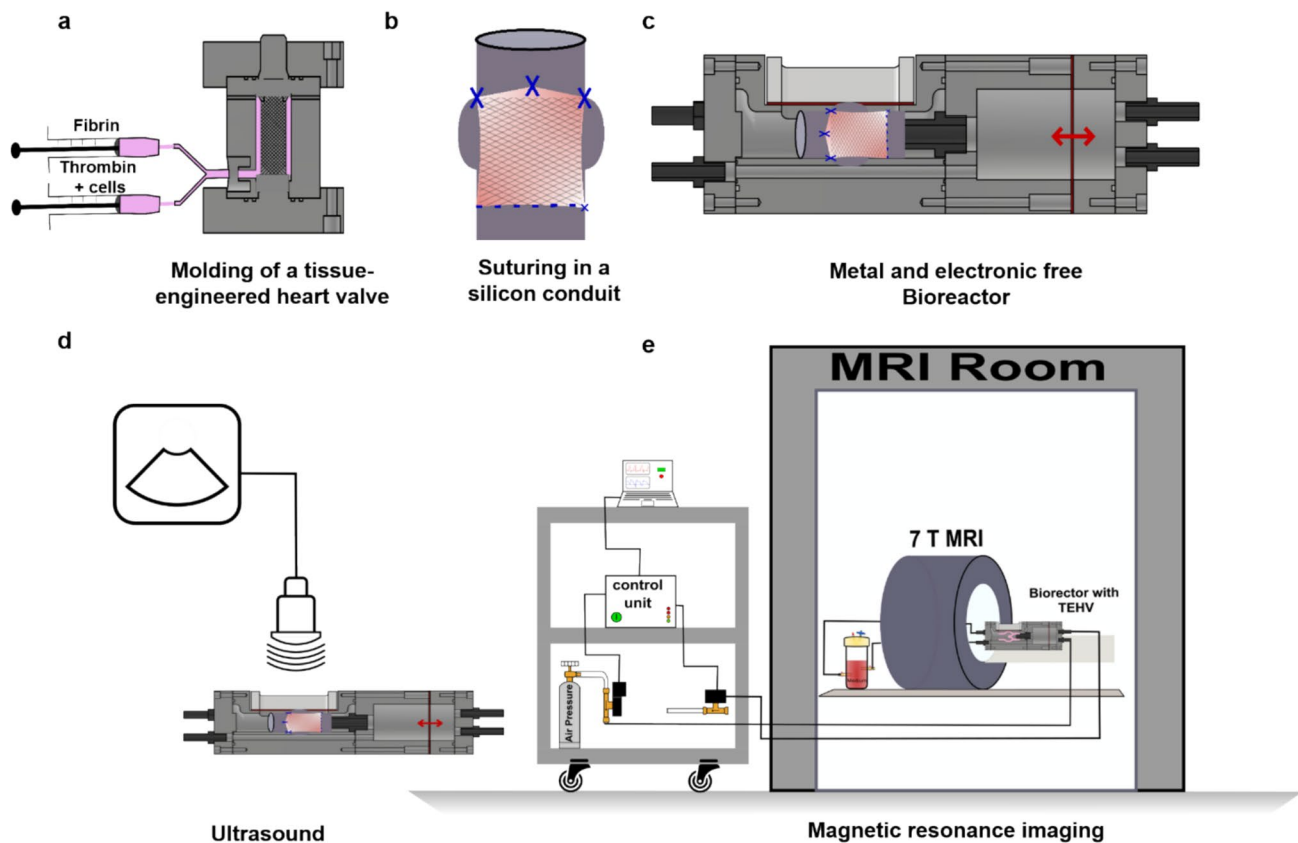


Fig. 1 Study design. **a** Molding of a tissue-engineered heart valve with the combination of fibrin, thrombin, and arterial smooth muscle cells. **b** Tube-in-tube-like structure and suturing of the heart valve

inside a silicon conduit. **c** Setup of the metal and electronic free bioreactor. **d** Ultrasound setup for the bioreactor. **e** Bioreactor and its elongated setup outside the MRI room

MRI motion artifact compensation and ultrasound imaging techniques. Furthermore, our bioreactor's role in enhancing extracellular matrix (ECM) production within the TEHVs by mimicking the physiological conditions of the human body by precisely controlling factors like fluid flow, temperature, CO₂ concentration, and pressure within the bioreactor was confirmed through immunohistological analysis, revealing abundant collagen, α -smooth muscle actin (α -SMA), and endothelial cell monolayers across the valve cusp.

Where ultrasound offers real-time insights into structural aspects and immediate changes, and MRI complements the analysis by providing detailed anatomical and functional information over longer timeframes, the synergy between these two imaging modalities enhances the overall understanding of tissue development, allowing researchers to make informed decisions during the design and optimization of tissue engineering strategies. In addition, this setup can also be transferred to translational implant development and enable an entire implant life-cycle management to ensure patient safety. Looking ahead, this bioreactor serves as a 'Blackbox' capable of gathering and interpreting critical information such as ECM remodeling and material

degradability, previously unknown, thus advancing our understanding of implant performance and longevity.

Materials and Methods

Production of Textile Mesh

The tubular textile mesh was produced from medical-grade polyethylene terephthalate (PET) multifilament yarn on a DR 16 EEC/EAC double-face Raschel warp knitting machine (Karl Mayer GmbH). The yarn had a yarn count of 78 dtex and consisted of 24 filaments. The yarn type was Fully Drawn Yarn (FDY) with 100% PET composition, and the breaking load of the yarn was 334 g, and the breaking elongation was 30%. A tull-filet pattern was employed while manufacturing, along with a needle gauge of E30 (equivalent to 30 needles per inch) and a course density of 15 stitches per centimeter. To create the tubular structure, 52 PET yarns were processed, and this structure was thermostabilized at 200 °C for 8 min on a metal rod before it was ready to be molded.

Electrospinning of SPION-Labeled PLGA Fibers

Poly(lactic-co-glycolic acid) (PLGA) (Purasorb PLG 8523, Corbion Purac Gorinchem, Netherlands) was dissolved in chloroform and methanol. The SPION particles were synthesized as described in Ref. [30] and were then mixed for 24 h with the PLGA solution at room temperature. The combination of both PLGA and SPION solution was loaded into a coaxial electrospinning needle (Bioinicia SL, Paterna, Spain) and was electrospun for 10 min in a custom-made device. Electrospinning was performed in a constant climate chamber (Binder GmbH, KBF 720) at 25 °C and less than 30% humidity. The motor for the rotation was applied to the platform for horizontal movement. The mandrel with the PET textile was attached to it via a PEEK (polyether ether ketone) connector. A plastic holder on the open side stabilizes the mandrel. The aluminum mandrel (13- and 15-mm diameter) and PEEK connector were custom-made. For each sample, a 15-cm-long PET mesh was set on the collector rod for spinning. The stand-off distance between the collector and nozzle tip was set to 20 cm, and the motor speed was 30 mm/s. The flow rates at the core were 0.5 ml/h and at the shell 1 ml/h during the spinning process. At the nozzle, + 22 kV (emitter) and the collector, − 20 kV, were applied during the spinning.

Scanning Electron Microscopy

For a comprehensive qualitative analysis of the fiber orientation, scanning electron microscopy (Thermo Fisher Scientific Inc., Quattro S) images were taken. The samples were coated (Leica Camera AG, High Vacuum Sputter Coater, EM SCD 500) either by gold palladium or graphite to prevent the charging of the surface. The operating voltage was set to 10 kV. Images were taken at 100-, 500-, and 1000-fold magnification. A gold–palladium coating was employed to enhance the signal-to-noise ratio during secondary electron detection mode (SE). To mitigate charging effects and guarantee electrical conductivity, a thin layer of Au/Pt was applied to the specimens before conducting SEM image measurements. SE mode images were captured with an electron acceleration voltage of 10 kV, utilizing an Everhart–Thornley detector (ETD) in a high vacuum setting at a distance of 15 cm. The precautionary step of coating the specimens with a thin layer of Au/Pt was taken to prevent charging effects and ensure optimal electrical conductivity during the SEM image measurement process.

Cell Isolation

Smooth muscle cells and endothelial cells were isolated from human umbilical cords under the approval of the ethics committee of the human subjects (vote of the local

ethics committee: 'EK 2067'). A transport buffer solution was prepared to transport the human umbilical cord. The umbilical cord was kept at 4 °C for 4 h before the isolation in the transport buffer. To remove the remaining blood clots, the umbilical cord was thoroughly cleaned with PBS via an irrigation cannula. The two arteries from the umbilical cord were harvested, and all the unwanted tissue was removed carefully with tweezers. As described before [11, 31, 32], for the collection of smooth muscle cells, the arteries were extracted from the cord and finely chopped into small ring-shaped sections using a scalpel. These small segments were then evenly distributed horizontally within a T75 cell culture flask. Once the arterial rings were slightly dry and stable on the surface, they were fed with fresh DMEM medium (Thermo Fisher, Germany) containing antibiotics. Since the flask was not coated with gelatin, it was unsuitable for endothelial cells, which were washed away during the medium change the following day. Small colonies of SMCs were observed in 2 to 3 days, and 70–80% confluency was achieved in 7 to 10 days.

To isolate endothelial cells, the lumen of the HU artery was filled with collagenase (Thermo Fischer, Germany) by a cannula and incubated at 37 °C for the collagenase enzymatic reaction to happen for 30 min. Following the removal of collagenase, the cells were cultured in a flask and supplied with an endothelial basal medium (Promocell, Germany). The flasks were coated with gelatin, which was responsible for cell attachment to the surface. Cell colonies were confirmed the following day, and confluency was achieved in a week.

Design and Production of the Bioreactor

The bioreactor was designed using computer-aided design (CAD) software (Autodesk, California, USA) and produced from polymethyl methacrylate (PMMA) by CNC machine. The bioreactor was divided into three distinct chambers, each designed for a specific function (Fig 2c). The first chamber, known as the fixation chamber, was where the TEHV was fastened. This chamber operated analogously to the ventricle of the heart, simulating the conditions that the valve would experience *in vivo*.

The second chamber, referred to as the observation chamber, functions similarly to the aorta of the heart. It includes an ultrasound window, which allows for real-time monitoring of the valve. In addition, MRI images were captured from this chamber, providing detailed insights into the valve's performance, hence its designation as the observation chamber.

The third chamber, the air chamber, contained only compressed air and no other medium. The pressurized air in this chamber exerts a force on a membrane, which in turn propels the medium from the fixation chamber

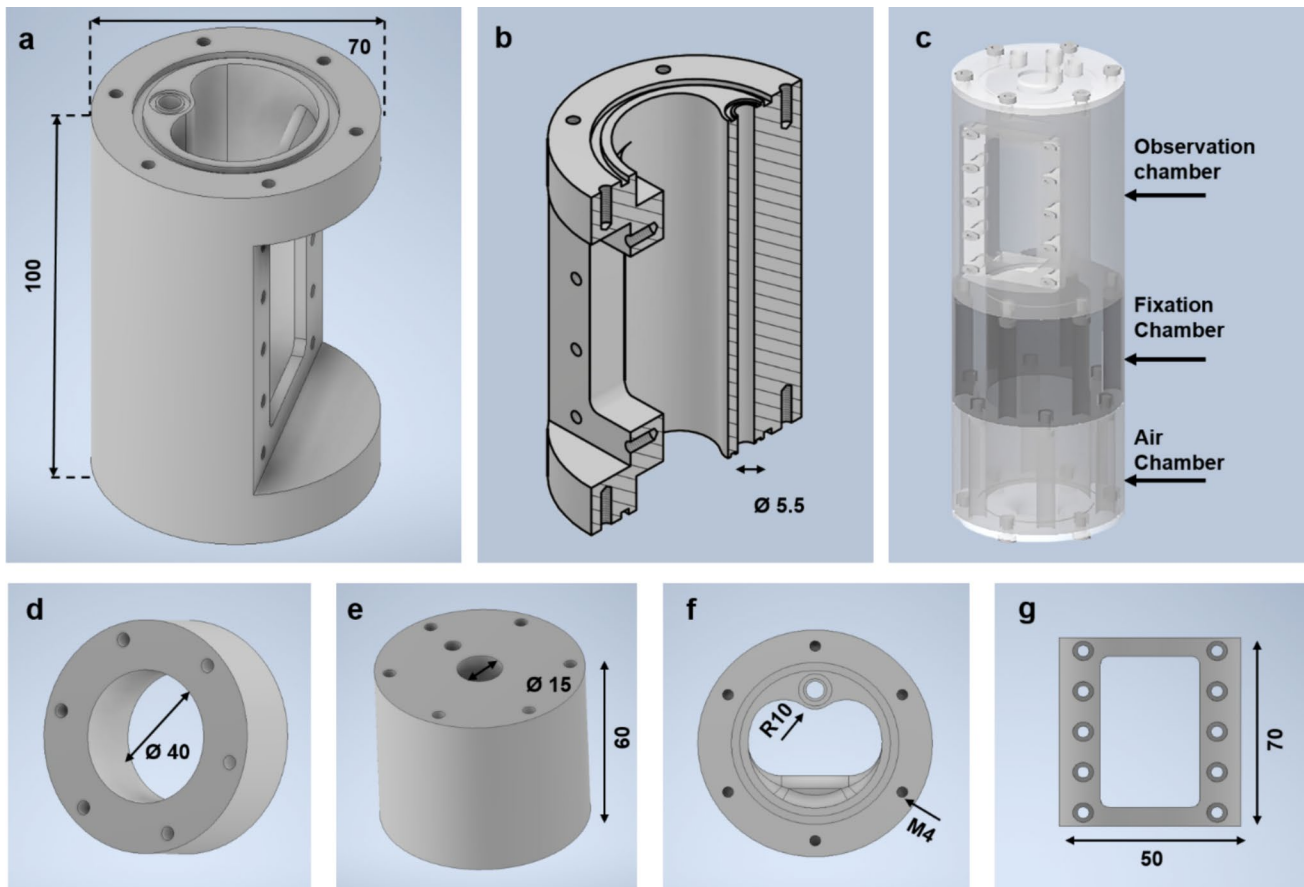


Fig. 2 Computer-aided design of the bioreactor chambers. **a** The observation chamber with an integrated backflow. **b** Side view of the observation chamber showing the vertical cross-section. **c** Assembly

of all chambers of the bioreactor. **d** Side view of air chamber. **e** Side view of fixation chamber. **f** Top view of the observation chamber. **g** The ultrasound window cap. All the dimensions are in mm

through the TEHV, effectively simulating the flow of the medium through a heart valve. All chamber's outer diameter was set to 70 mm as the coil in the MRI system had a 72 mm diameter. The inner diameter of each chamber was designed according to their different application, as mentioned in Fig 2a, d, and e.

The transparent nature of PMMA makes it suitable for qualitative observations of the conditioning. All parts of the bioreactor except the screws and membrane were sterilized by low-temperature hydrogen peroxide gas plasma (ASP Global Manufacturing GmbH, STERRAD 100S Sterilization System). To assemble all the chambers of the bioreactor, 20 M4x20 and 10 M4x8 polyether ether ketone (PEEK) and 6 M4x50 polyamide PA screws were used. Pieces of silicone membrane (thickness 0.44 mm) (Wacker Chemie AG) were cut to fit between the air and fixation chamber and between the observation chamber and observation window (Fig. 2g).

To avoid leakage, sealing rings were inserted at the contact areas of the remaining bioreactor parts. Three and two nozzles (Sang-A, straight hose nozzle 8 mm R 1/8" male thread PA) were added on the lid and the floor, respectively.

The threads of the nozzles were covered by Teflon film to prevent leakage.

Tissue-Engineered Heart Valve

Two cylindrical structures were engaged to make the TEHV. One is a silicon conduit that acts as a housing of the valve, and another is a tubular scaffold, which is the leaflets. This structure is based on a tube-in-tube concept, where the leaflets were stitched into a silicone housing conduit (Fig 1b). The valve was molded in a 3D-printed veroclear mold where the hydrogel and cells were injected (Fig 1a, S1). The hydrogel matrix was prepared by combining 50% fibrinogen (10 mg/mL), 7.5% thrombin (40 U/mL), 7.5% 50 mM CaCl₂ in Tris buffer solution (TBS), and human umbilical artery smooth muscle cells. The cell density was 10×10^6 cells/mL in a total 2 mL volume of fibrin gel for every valve. After the injection molding and the fibrin gel were allowed to polymerize completely, the TEHVs ($n=3$) were statically conditioned for 7 days, following the procedures outlined by Moreira and Weber [29]. During this static phase, the

culture medium is continuously cycled through a reservoir with gas exchange filters, ensuring a stable environment for the cells, although the valve is not yet exposed to dynamic flow conditions. This static conditioning phase is crucial for the initial growth and maturation of the ECM, making the valve more resilient and better prepared to withstand the stresses of dynamic flow introduced later in the process.

After the static culture, the valves were endothelialized inside a 50 mL falcon tube with an endothelial cell density of 3×10^6 /mL. To culture, both endothelial cells and smooth muscle cells, a combination of both mediums was used along with supplements. The bioreactor medium consisted of 500 mL of DMEM along with 50 mL fetal bovine serum, 5 mL antibiotics, 308 mg Vitamin C, and 1712 μ L tranexamic acid, and 500 mL of Lonza EGM (Lonza Group AG, EGM-2 Microvascular Endothelial Cell Growth Medium-2 BulletKit, CC-320) with supplements and 308 mg of Vitamin C. The bioreactor runs for 7 days and is driven by a pressurized air system. A magnetic controllable valve (ODE-Magnetventile/SFS-Fluid Systeme GmbH, magnetic valve, 21A2ZV45D) was connected to a pressured air supply that provides a pressure of 1 bar and to the nozzle on the floor of the bioreactor. The second outlet of the air chamber is connected to a second controllable valve (ASCO Power Technologies, microfluidic valve, PVG202A203V.24/DC), which has an open end on the other side. Both valves were connected to a DAQ box to control the valves via the LabView program.

The bioreactor is positioned within an incubator maintained at 37 °C and a CO₂ concentration of 5% (CB 210, BINDER GmbH, Germany). The bioreactor culture medium was manually changed every 3 days.

Magnetic Resonance Imaging

The bioreactor setup was the only component placed inside the MRI room (Figs. 1e, 5a), with all electronic equipment and controls kept outside to avoid interference with the MRI. Compressed air required for the valve's operation was delivered through specific air-pressure-carrying tubes, which connected the external air supply to the bioreactor inside the MRI room. This arrangement ensured that the bioreactor could function effectively within the MRI environment without compromising the imaging quality or the integrity of the electronic systems.

TEHVs were monitored using a Bruker BioSpec 70/20 USR 7 T MRI scanner (Bruker BioSpin GmbH, Germany). To reduce movement artifacts, a breathing patch was secured on top of the ultrasound membrane to synchronize MR data acquisition to the mechanically induced cardiac cycles. First, the positioning and the MRI visibility of the valve were assessed by T2-weighted sequences, which were acquired axially and coronally using a fast spin

echo sequence [repetition times (TR): 209.4 ms; echo time (TE): 2.8 ms; flip angle: 50°; averages: 4; matrix size; 360 x 360; field of view (FOV): (50 x 50) mm²; slice thickness; 1 mm]. Subsequently, gradient-recalled echo pulse or cine sequences of the heart valves, consisting of multiple static images rapidly displayed in a continuous loop, were acquired [TR: 11.02 ms; TE: 3.9 ms; flip angle: 10°; repetitions: 4; oversampling: 100; movie frames: 15; matrix size; 256 x 256; FOV: (50 x 50) mm²; slice thickness; 1 mm]. Imalytics Preclinical Software (Gremse-IT GmbH, Aachen, Germany) was employed for image analyses. The maximum opening area of the valves was calculated using the Image J (NIH, USA) software.

Ultrasound

Ultrasound was performed using a VEVO 3100 ultrasound system equipped with a linear array-MX-250 transducer (FUJIFILM VisualSonics, Toronto, Ontario, Canada). The transducer was placed vertically onto the bioreactor window positioned on top of the heart valves. The small cavity of the US window was filled with water to decrease the acoustic impedance. The heart valves were imaged in bright field mode at 21 MHz frequency and 100 frames. VevoLAB software version 5.2 (FUJIFILM VisualSonics, Toronto, Ontario, Canada) was used for image analyses.

Immunohistochemistry

The Carnoy's solution was used to fixate the samples based on the previously published protocol described by Koch et al. [33], which is a mixture of ethanol, chloroform, and acetic acid. Afterward, the samples were washed in ethanol for 30 min, followed by dehydration using a dehydration device (Leica TP 1020, Wetzlar, Germany). The specimens were subsequently embedded in paraffin for storage until further use. Sections of paraffin, with a thickness of 5 μ m, were cut using a microtome (PFM medical, Germany). Preceding the staining process, the samples underwent deparaffinization through a sequential dilution series of xylol and ethanol. The Sequenza Staining racks (ThermoFisher Scientific, Massachusetts, USA) were employed to secure the samples in position. To block and permeabilize the tissues, a 0.1% Triton X-100 aqueous solution containing 5% normal goat serum (NGS) from (Agilent Dako, Santa Clara, California, USA) was utilized. Subsequently, the primary antibodies were subjected to an incubation period at 37 °C for 1 h, followed by a triple wash with PBS for 5 min each. The samples were incubated with the corresponding secondary antibodies for 1 h. Following another round of triple washing, the samples were incubated with DAPI (1:500) from (ThermoFisher Scientific, Massachusetts, USA), washed three times with PBS, and finally mounted using a fluorescent mounting medium from

(Agilent Dako, Santa Clara, California, USA). The primary antibodies utilized for the histological analyses were directed against anti-human CD31 (Sigma-Aldrich, Darmstadt, Germany), anti-human alpha-smooth muscle actin (α -SMA) (Sigma-Aldrich, Darmstadt, Germany), and anti-human type I collagen (Acris Antibodies GmbH, Herford, Germany). The secondary antibodies, namely anti-mouse Alexa Fluor 488 and anti-rabbit Alexa Fluor 594, were sourced from Thermofisher Scientific (Massachusetts, USA). The immunohistology images were acquired using an Axio Imager M2 fluorescence microscope (Carl-Zeiss, Oberkochen), with a magnification of 5x for the overview of the cusp and 20x for the detailed image of the cusp.

Results

Electrospinning and Molding of the TEHVs

The PET textile scaffold and the non-woven electrospun fibers from the SPION-labeled PLGA were visible under a light

microscope (Fig 3a, b). However, to observe the orientation and deposition of the fibers, scanning electron microscopy (SEM) was performed. The SEM images (Fig 3d) confirmed the uniform fiber distribution and the porosity achieved with the electrospun coating. No evidence of fiber agglomeration was found. The porosity of the PET scaffold was calculated by area measurement in a microscope (Keynce, Offenbach, Germany). The porosity was 49.5% in the textile scaffold ($n = 3$, $SD = 0.47$).

Bioreactor Design and Setup

The limited space imposed by the 72-mm diameter MRI coil prevented the inclusion of peripheral tubing, which is essential for ensuring a connection between the ventricular and atrial block. Consequently, an integrated backflow system was successfully designed to circumvent this need for peripheral connection (Fig 2a–c). As shown in Fig 4d, the whole bioreactor appears as a single cylinder because the connection between the ventricular and aorta block was fully integrated, which successfully resulted in placing the

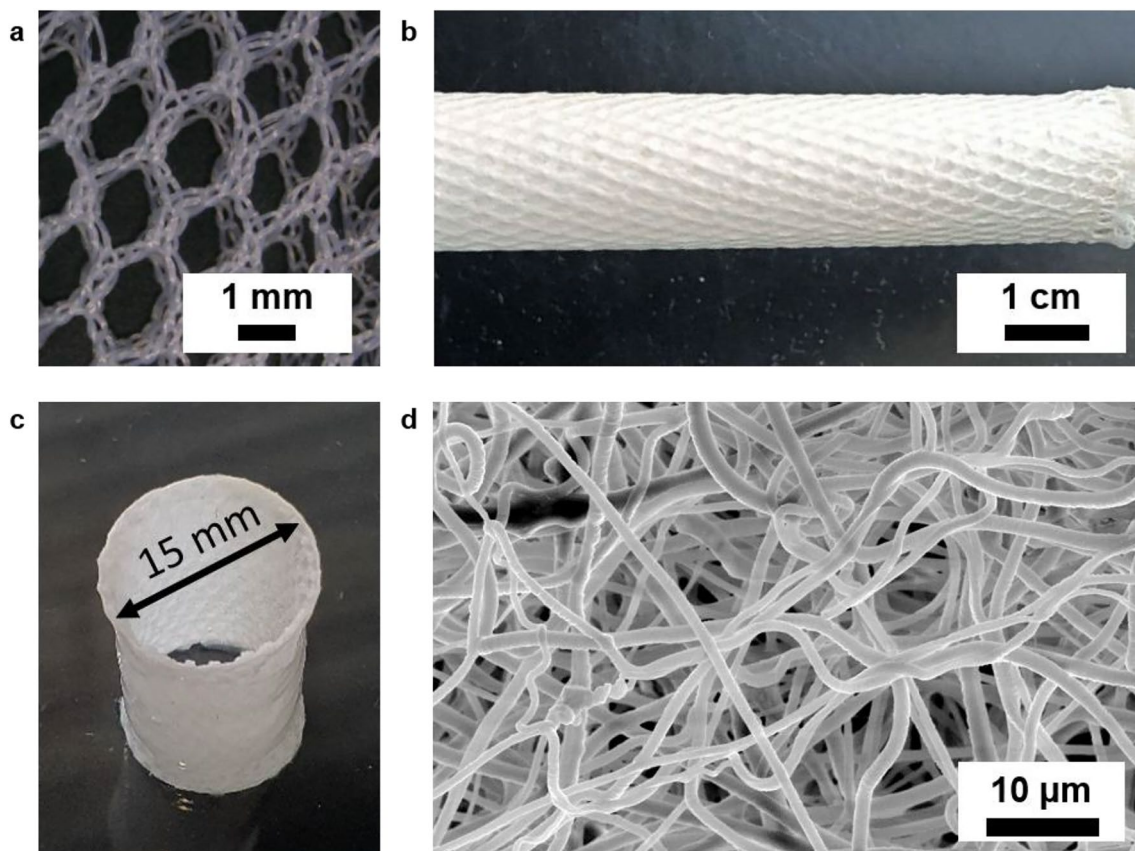


Fig. 3 Textile mesh and the electrospun coating. **a** Wrap-knitted PET textile mesh showing the multifilament threads and tulle-like pattern. **b** The textile scaffold after electrospun coating by SPION-labeled PLGA solution. **c** A molded tube of fibrin, thrombin, and cells before

it is placed and sutured inside the silicon conduit. **d** Scanning electron microscopy of the electrospun fibers representing the fiber distribution

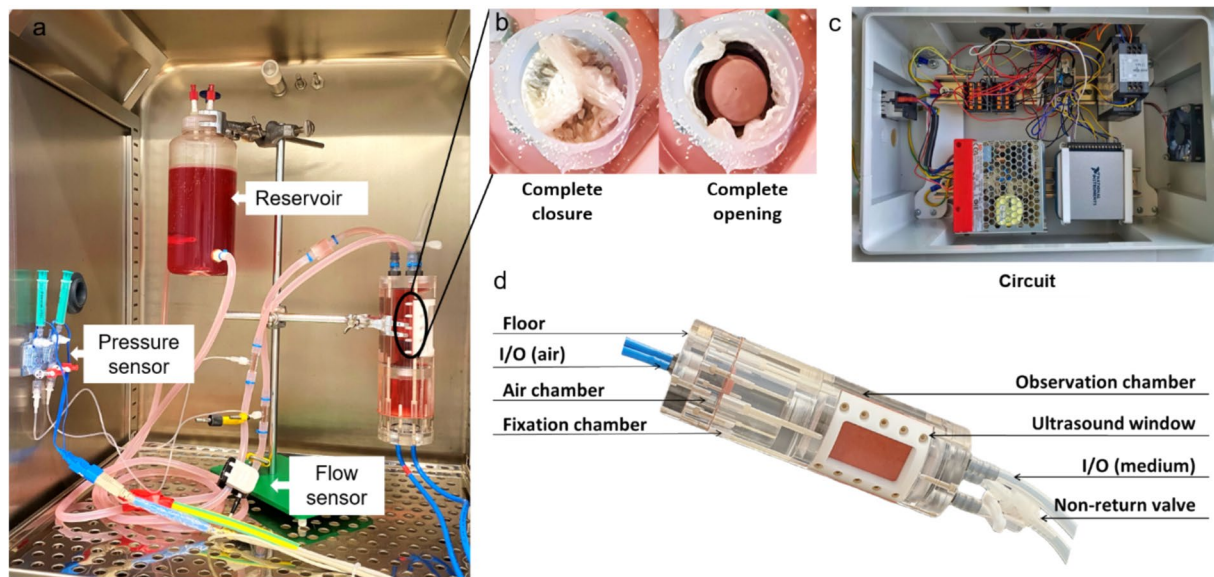


Fig. 4 Bioreactor setup with circuits. **a** The bioreactor setup inside the incubator shows the components like the pressure sensor, flow sensor, and pneumatic drive channels. **b** Representative pictures of the complete opening and closing of the valves when observed from

the top. **c** The circuit and data acquisition (DAQ) device that runs the bioreactor. **d** The assembly of the bioreactor shows the chambers and their fittings

bioreactor in the MRI coil. The bioreactor was designed to have an outer diameter of 70 mm to fit in the MRI coil and have 1 mm on each side for free movement.

The cardiac cycle was represented in two phases: during the diastolic phase, as the membrane moved downward, the cell culture medium flowed from the ‘atrial’ reservoir into the ‘ventricular’ chamber of the bioreactor, passing through a non-return valve that mimicked the mitral valve function. In the subsequent systolic phase, the membrane was pneumatically pushed upward, displacing the medium through the ‘aortic’ valve into the ‘aorta’, and from there, it returned to the atrial reservoir, which also acted as a windkessel, simulating aortic compliance.

The closed-loop bioreactor system (Fig 4a) did not show any leakage. The mechanical valves of the pressurized air system were reliable. The tubing system between the bioreactor and medium reservoir tended to collect air, which was then removed manually afterward. The complete opening of the TEHV was achieved by considering three important factors: (1) the amount of pressure supplied to the air chamber, (2) geometry, and (3) the suturing positions of the valve. In our *in vitro* experiments, valves opened fully at a ventricular pressure of 20–40 mmHg.

Magnetic Resonance Imaging

Upon placing the bioreactor within the MRI coil (Fig 5a), the initial localizer MRI sequence revealed the placement of the valve and the designated imaging area of interest (Fig

5b). Gated MRI ensured that the images were acquired at consistent and predetermined points in the cardiac or respiratory cycle, allowing for clearer and more accurate visualization of moving heart valves (Fig 5e, f). The breathing patch (Fig 5c) was utilized in this study to detect the cardiac cycles of the TEHV, which were imposed by the pressure supplied through the air chamber. This enabled the performance of gated MRI, which is fundamental for minimizing motion artifacts and obtaining high-quality images. Consequently, the MRI image acquisition was synchronized to the breathing rate, which was set to 70 per minute (Fig 5d).

For qualitative analysis of TEHVs, T2-weighted images were acquired in coronal, sagittal, and axial planes, successfully showing the positioning and dynamic function of the valve (Fig 6a–f). The maximum valve opening area was calculated in comparison to the area of the silicon conduit. The average opening area of the TEHVs ($n=3$) was determined to be 71% (108.78 mm^2) when measured from axial MR images (Fig 6c) and 77% (122.82 mm^2) when measured from sagittal MR images (Fig 6f). These measurements were taken by comparing the opening area to the original diameter area of 15 mm. The standard deviation was 0.85 for the axial measurements and 3.08 for the sagittal measurements. All the samples were tested on day 7 of the dynamic conditioning. These sequences were acquired in both axial and coronal orientations employing a fast spin echo sequence, and this detailed approach provided a comprehensive assessment of the valve’s spatial orientation and visibility within the MRI.

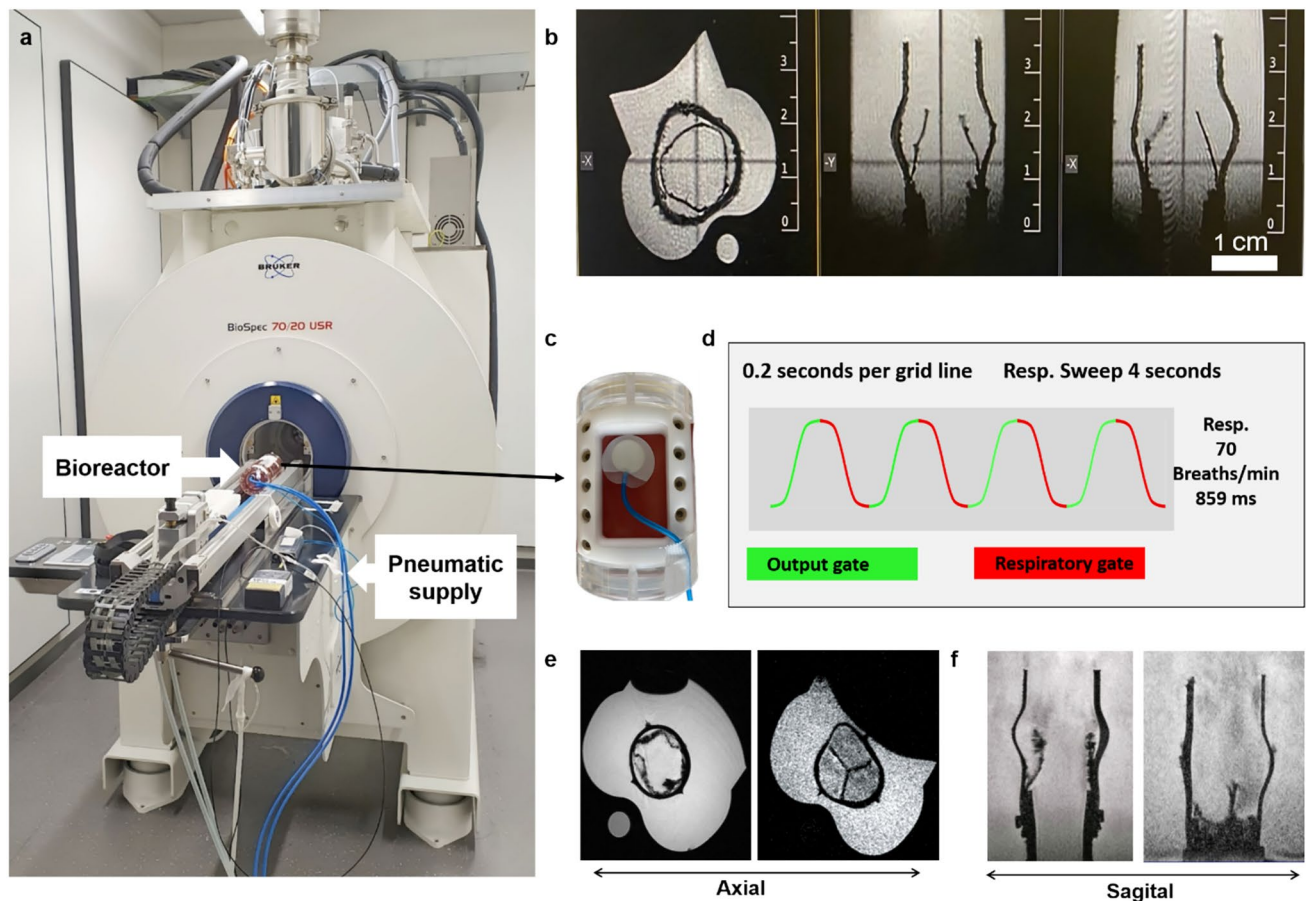


Fig. 5 Dynamic magnetic resonance imaging. **a** The bioreactor going inside the 7 T MRI coil and the blue tubes are the inlet and outlet of pneumatic connections. **b** Localizer sequence shows the placement of

the valve in MRI. **c** The breathing patch on the top of the ultrasound window. **d** The respiratory graph observation during the MRI scans. **e–f** Observation of the opening and closing of the valve in the MRI

By analyzing the forward and backward volumes during single cycles and calculating the regurgitation factor in accordance with ISO 5840-1, we determined that the regurgitation factor was 12.29% ($n = 3$, $SD = 0.85$).

Following this initial examination, we further refined our evaluation by employing gradient-recalled echo pulse sequences, commonly known as cine sequences, specifically focusing on the heart valves. These sequences consist of multiple static images that were rapidly displayed in a continuous loop, offering a dynamic portrayal of the cardiac valves. The imaging approach allowed us to capture intricate details of the heart valves in motion, facilitating a comprehensive understanding of their dynamic behavior and structural integrity.

Ultrasound

The dynamic functionality of TEHVs within the bioreactor was comprehensively tracked using brightfield-mode ultrasound, as depicted in Fig. 6g–i. The transducer was

positioned vertically above the ultrasound window, which was a membrane located 2 cm from the heart valves. To reduce acoustic impedance, the small cavity between the membrane and the outer area of the ultrasound window was filled with water. Gray scale values at the opening frames were measured at 144.41 ± 33.42 (a.u.), and at closing frames, they were measured at 164.5 ± 37.55 (a.u.). This imaging modality facilitated qualitative observation of the opening and closing cycles of the TEHVs, providing valuable insights into their dynamic performance.

Immunohistochemistry

The results of immunohistological staining displayed the expression of collagen I and smooth muscle actin throughout the cusp of the valve, particularly in close proximity to the nuclei (Fig 7a–c). A monolayer of endothelial cells was found on the border of all the TEHV cusps evidenced by CD31 staining (Fig 7b). Furthermore, the TEHVs were qualitatively compared with native porcine aortic heart valves

Fig. 6 MR and ultrasound imaging of the TEHVs. **a–c** Axial views of the TEHVs in both T2-weighted, cine sequence, and maximum opening area. **d–f** Sagittal view of the TEHVs in both T2-weighted, cine sequence, and maximum opening area. **g** The bioreactor setup is on the ultrasound bench where the transducer is on a movable axis. **h** Opening frame of the TEHVs. **i** Closing frame of the TEHVs

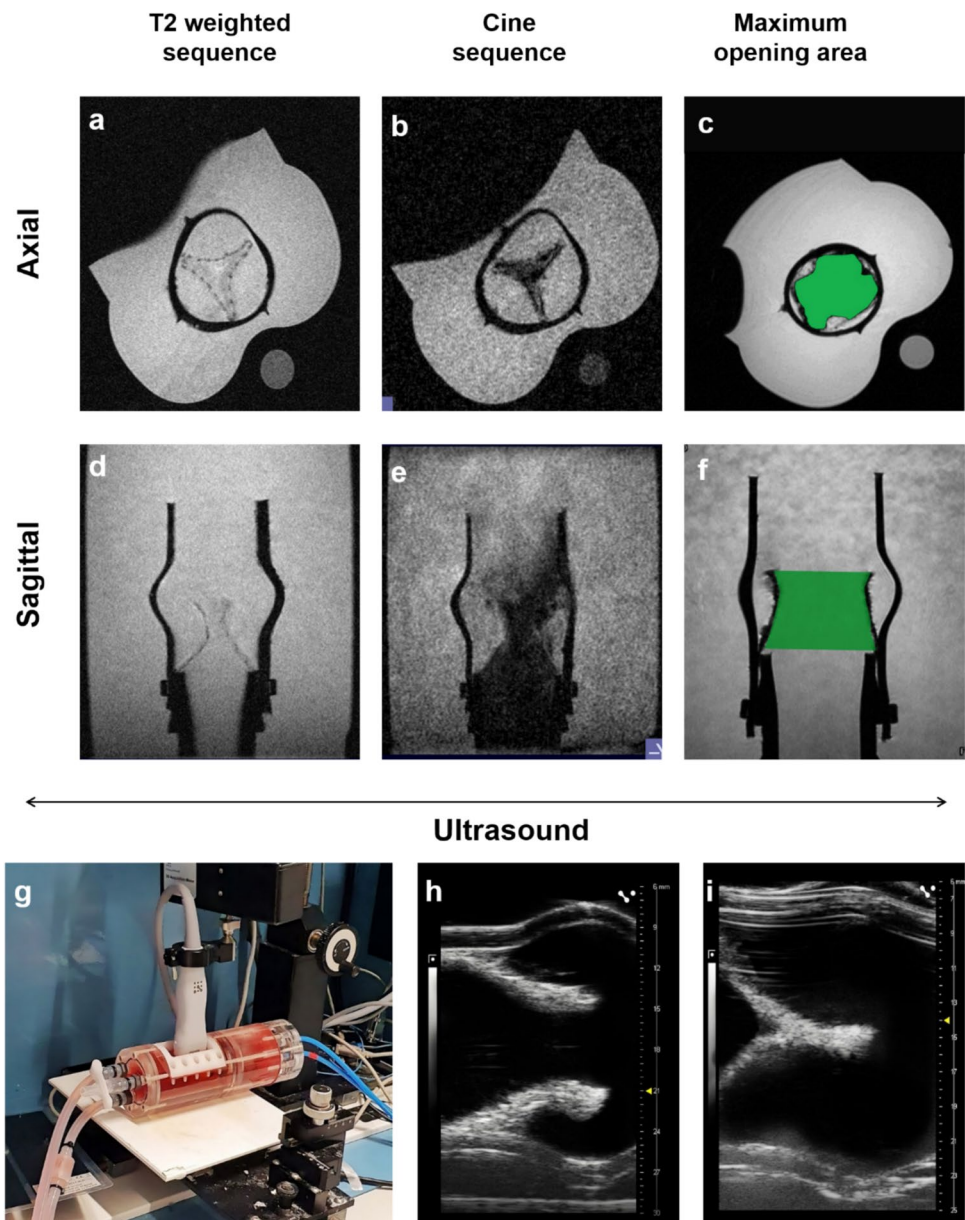


(Fig 7d–f). The TEHVs were not negatively affected by the electrospun coating of SPION-labeled PLGA.

An overview observation of the entire cusp of the TEHV shows two different types of cell density areas. The first one, as depicted in Fig 8a, shows the area where the hydrogel was present, and the second type (Fig 8b) shows the area where the multifilament textile was present.

Discussion

In this study, we designed and constructed a bioreactor with a focus on magnetic resonance imaging (MRI) and ultrasound (US) compatibility. This was achieved

by refraining metal components, integrating backflow design, and incorporating a US-compatible membrane, enabling comprehensive imaging of implant behavior without interference. We produced small tissue-engineered heart valves (TEHVs) with a 15 mm diameter, with a specific focus on research for young patients. The TEHVs were produced using polyethylene terephthalate (PET) as the non-degradable backbone of the textile scaffold, poly(lactic-co-glycolic acid) (PLGA) as the biodegradable and biocompatible textile component, and fibrin gel containing smooth muscle cells (SMCs) and endothelial cells (ECs). The TEHVs were dynamically conditioned in a custom-made MRI-compatible bioreactor (Fig. 4, S2) and monitored using MRI and ultrasound imaging, with a

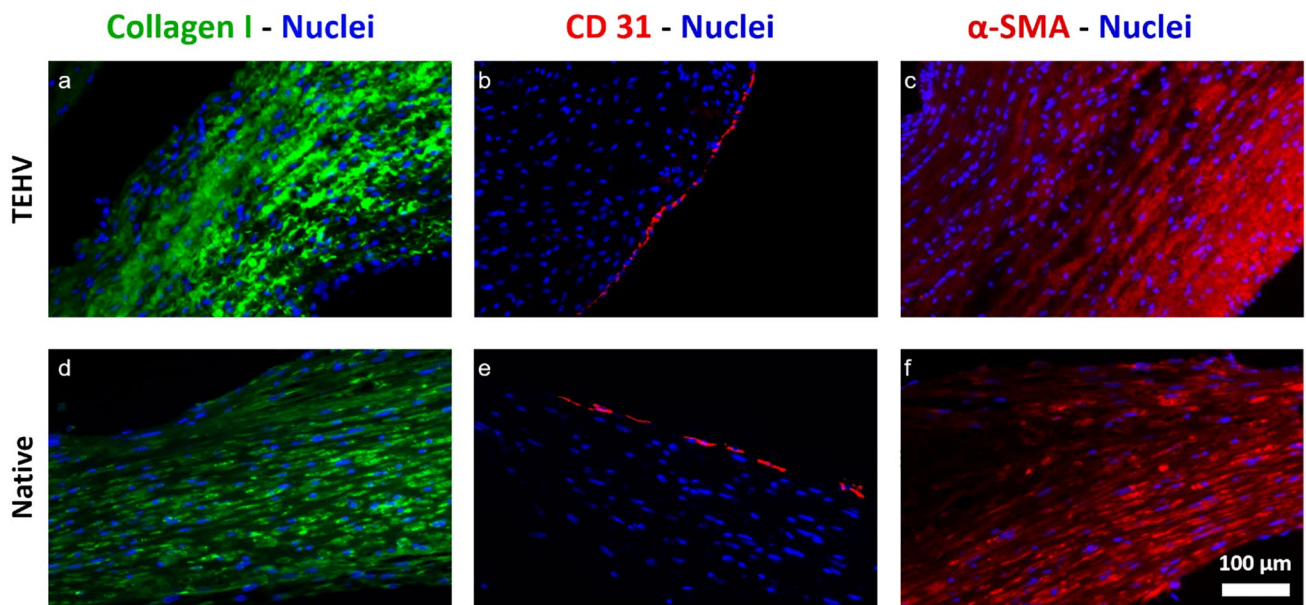
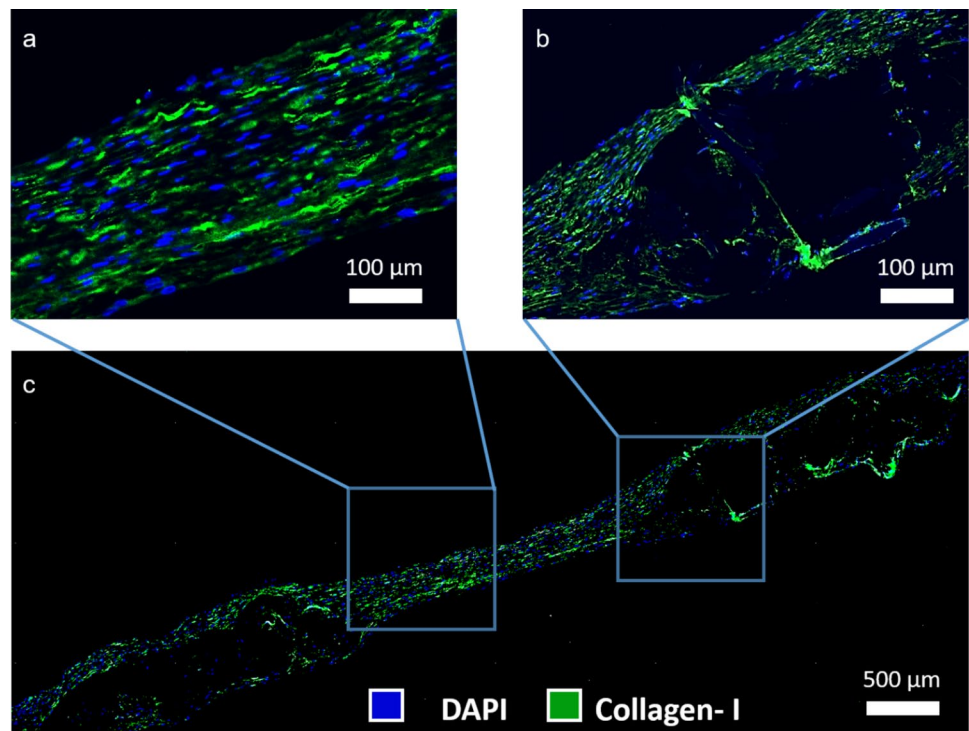


Fig. 7 Immunohistology analysis of the TEHVs in comparison to porcine aortic valve. **a–c** Nuclei (blue), collagen I (green), CD31 (red), α -SMA (red). **d–f** Porcine aortic valve as native control

Fig. 8 Cell distribution over the cusp. **a** Cell dense areas of the TEHVs. **b** Multifilament textile areas. **c** Overview of the TEHV cusp



focus on assessing implant safety and optimizing life-cycle management.

Several heart valve bioreactors have already been reported in the literature. For example, Amadeo et al. showed a heart valve bioreactor consisting of a decellularized porcine pericardium, in which they were able to achieve successful cell

seeding. However, this model was a perfusion-assisted bioreactor, and the achieved flow of 0.03 ml/min is not an optimal human diastolic blood flow rate. The perfusion syringe contained 6 ml of medium, which was changed every 72 h, which is also not an appropriate volume to functionalize a heart valve [34]. A similar attempt was made by Ott et al.

with decellularized rat hearts cultured in a perfusion bioreactor system under organ culture conditions [35]. Several other studies reported the use of functional bioreactors to condition heart valves [16, 36]. However, to advance heart valves toward clinical implementation, there is a critical need for robust, longitudinal, non-invasive analysis that can ensure safety and facilitate regulatory approval processes more effectively.

In the present work, we built on our previous efforts where we used the concept of biohybrid tissue-engineered constructs, which consist of fibrin, human cells, and a non-degradable textile scaffold [9, 11]. PLGA fibers were additionally labeled with SPIONs to enhance MRI visibility of the valves and allow for dynamic monitoring of their complex movement. PET was chosen as the scaffold due to its proven biocompatibility, uniformity, mechanical strength, and abrasion resistance [37]. Similarly, PLGA was selected for its proven biodegradability and biocompatibility [38]. Furthermore, the degradation rate of PLGA can be precisely controlled by adjusting the lactic-to-glycolic acid ratio, providing additional flexibility in tailoring the coating's lifespan to suit specific clinical requirements. This versatility, combined with PLGA's well-established safety profile and mechanical properties, made it the most suitable choice for our coating application, especially when compared to slower-degrading polymers [39, 40].

Upon production, the heart valve undergoes conditioning within a bioreactor (Fig 4d), facilitating optimal flow while regulating pressure and temperature. This bioreactor is meticulously engineered to provide electronic feedback (Fig 4c) through integrated sensors. Moreover, non-invasive imaging techniques are employed to dynamically visualize its function. In our current study, we present the design of a bioreactor with dual objectives: first, to foster tissue maturation in a tissue-engineered heart valve, and second, to enable observation of the valve via MRI and ultrasound modalities.

In the clinic, aortic valve diseases are diagnosed by echocardiography, CT, ultrasound, and MR imaging, which also need to be studied thoroughly in research to observe the remodeling. For tissue conditioning in TEHVs, an adequate environment and specific process parameters are essential. To monitor the conditioning TEHVs, a heart valve bioreactor is equipped with multifunctional setups like motors, pressure sensors, flow sensors, temperature sensors, and many more tubular connections for input and output supply. However, this complicated setup generally contains electronic instruments and metal-containing devices, making it a bottleneck to perform MRI. The characterization of implants through molecular imaging provides the most suitable tool to study implant behavior before they go to transplantation [41]. Backflow is critical in heart valve bioreactors as it affects valve efficiency and durability by simulating physiological regurgitation. We have installed a non-return valve (Fig 4d)

to prevent the medium from flowing back into the chamber. By analyzing the flow profile, we calculated the regurgitation factor to be approximately 12.29%. In the future, we plan to apply Doppler flow data to analyze our regurgitation using the ultrasound membrane window in our system.

Bioreactors with mechanical pistons and motors with gear head assembly were also reported before by Miller et al. [42], which could cause the opening and closing of the valve but limited monitoring and molecular imaging ability. Voss et al. and Moreira et al. produced bioreactors with ultrasound windows but involved actuators to move the membrane, for which the MR imaging ability was restricted [24, 29]. We reported a pneumatic system where an elongated tube supplies the air pressure from outside the MRI room (Fig 1e, 5a). With the pneumatic system, the compressor and controller were kept outside the MRI room, and the compressed air reached the bioreactor, which avoided the metal and electronic interference with the MRI. Though the air pressure-actuated heart valve reactor was previously reported by Beelen et al, the bioreactor was very big and complex to get inside a 7 T MRI coil [43]. Furthermore, our integrated backflow design not only makes the bioreactor more compact but also circumvents geometric complexities. Initially, we attempted to fasten the bioreactor using brass and polyamide screws. However, we encountered challenges with brass screws producing artifacts in imaging and polyamide screws proving insufficient due to their low mechanical strength, leading to wear after a single use. This limitation prompted us to transition to PEEK screws, which offered superior mechanical properties and durability for sustained performance within the bioreactor system. The primary novelty of our bioreactor lies in its ability to dynamically image a heart valve under 7 T MRI, a feat that has not been previously reported. The 7 T MRI represents state-of-the-art technology, currently used only in preclinical testing due to its very small-bore diameter.

Our innovation addresses this limitation by designing a compact bioreactor that houses all necessary equipment internally without relying on external tubular connections between the ventricular chamber and aorta. We introduced an integrated backflow technology that allows the medium to circulate internally, enhancing functionality while fitting within the confined space of the 7 T MRI.

As shown in Fig 5b, the valves were initially scanned with the localizer sequence to bring them to the required position where the valve was visible. The static images were taken with the T2-weighted sequence, where the valves were studied qualitatively. Previously, we have proven static non-invasive imaging in tissue-engineered vascular grafts where the structure was enclosed with cylindrical silicon tubes [10, 11].

Compared to vascular grafts, heart valves are more complex and dynamic. Therefore, in the current study,

the dynamic movement was studied by executing a cine sequence where the valves could be seen moving, most importantly, the complete opening and closing (Fig 5e, f). Moreover, from a future perspective, MR fingerprinting (MRF) could provide enhanced tissue diagnosis, treatment monitoring, and tissue characterization. MRF is a new approach that allows simultaneous measurement of multiple tissue properties in a time-efficient manner by varying acquisition parameters, such as radiofrequency flip angle, TR, and k-space sampling trajectory [44].

Moroz et al. described how dynamic MRI could answer many clinical questions and allow the study of physiological properties in both normal and diseased tissue constructs [45]. We included a breathing patch (Fig 5c) at the ultrasound window membrane, which showed the breathing rate and allowed motion compensation to avoid motion artifacts. The breathing patch typically consists of a sensor or device placed on the patient's chest or abdomen to monitor respiratory motion. The information from the breathing patch is then used to trigger the gating of MRI sequences, ensuring that images are acquired at specific points in the breathing cycle. The heart valve's maximum opening area was observed to range from 70 to 80% compared to its silicone housing (Fig 6c, f), potentially influenced by the valve's smaller size (15 mm diameter). Effective suturing technique is critical for optimizing valve opening and closure dynamics, suggesting that enhancements in suturing methods could further improve performance. In healthy adults, the effective orifice area (EOA) of the aortic valve typically ranges from approximately 2.5 to 3.5 cm², which is essential for distinguishing normal valve function from pathological conditions [46, 47]. For prosthetic heart valves, the EOA varies based on the type of valve. For example, Firestenberg et al. reported EOAs ranging from 1.3 to 2.1 cm² for bioprosthetic valves [48], while Amarelli et al. found EOAs between 1.5 and 2.0 cm² for mechanical prosthetic valves [49]. Similarly, Buchanan et al. discussed transcatheter aortic valve implantation (TAVI) with EOAs also ranging from 1.5 to 2.0 cm² [50]. To express these values as a percentage of the fully open area of a normal valve, the following formula can be used: Opening Percentage = (Effective Orifice Area/Anatomical Orifice Area) × 100 [51]. For instance, if a patient has an anatomical orifice area of 3.5 cm², an EOA of 2.0 cm² would represent approximately 57% of the fully open area of a normal valve. Given that the anatomical area typically ranges from 2.5 to 3.5 cm², the percentage range for prosthetic EOAs would be around 37% to 84% of the normal valve's opening area.

The ultrasound results show that the TEHV could be observed and imaged dynamically (Fig 6 g–i). Though ultrasound imaging-assisted bioreactor has been found in the literature, the image quality was found to be distorted due to the thicker membrane and stand-off distance of the

transducer from the valve [24, 29]. Hurtado–Aguilar et al. previously constructed a PMMA bioreactor and utilized ultrasound probes to visualize TEHVs. However, the thickness of the reactor wall (ranging from 5 to 15 mm) led to compromised image quality [52]. To address this issue and achieve better visualization of the valves, we designed a dedicated ultrasound window featuring a 0.44 mm-thick membrane secured with PEEK screws (Fig 4d). The use of a 21 Hz transducer combined with a highly elastic membrane enabled easy localization of the valve and yielded high-quality images (Fig 6g–i). Ultrasound analysis, leveraging gray-scale values, offers insights into collagen distribution and formation. Kreitz et al. conducted an analysis correlating gray-scale values from ultrasound scans of cell-embedded fibrin gels with hydroxyproline content, demonstrating a strong association with collagen formation in heart valves, which was consistent with histological findings [53]. This approach can be applied within our bioreactor system and in future longitudinal studies to assess collagen propagation and provide valuable data on tissue development over time. Further, longitudinal studies are needed to assess whether our novel bioreactor model and selected conditioning parameters support in vitro ECM production and deposition, which could be non-invasively monitored by correlating ultrasound gray values with subsequent histological analysis.

The immunohistology analysis meets the hypothesis of having high cell density and high expression of collagen and smooth muscle actin. As depicted in Fig 7, TEHVs exhibit abundant collagen and smooth muscle actin production, with cellular and extracellular matrix (ECM) morphology comparable to that of the native heart valve when observed qualitatively. Further denser ECM can be achieved by prolonged bioreactor conditioning. Nevertheless, our objective is also tied to reducing the conditioning duration to expedite the availability of the valves in clinical settings. The heart valve cusp overview reveals two distinct tissue density regions, illustrated in Fig 8a–c, wherein one area exhibits high density while the other displays a wider blank space. To better understand the phenomena, Fig. 8c and Fig. 3 need to be compared, where the structure of the wrap knitted textile shows the gap between the fibers. The space between the fibers contained most of the hydrogel, which acted as a cell carrier, and the multifilament fibers caused the blank wide spaces in immunohistological analysis.

To summarize, the successful translation of TEHVs into clinical practice necessitates a comprehensive approach to monitoring their integration dynamics and long-term performance. Non-invasive and radiation-free imaging modalities emerge as indispensable tools in this endeavor, offering unparalleled insights into the implant's life cycle from fabrication through to patient follow-up evaluations. By implementing advanced imaging techniques alongside innovative tissue engineering and bioreactor setup

strategies, the implants can pave the way for safer and more efficacious solutions in cardiovascular regenerative medicine. Looking forward, the new bioreactor presents opportunities to explore a wide range of imaging applications for assessing ECM dynamics, scaffold degradation, and relevant markers, providing critical insights into tissue maturation and implant performance.

Our study introduces an innovative bioreactor capable of conditioning a biohybrid heart valve and facilitating multi-modal imaging, including dynamic imaging using a 7 T gated MRI and a 21 Hz ultrasound probe. The adaptation of integrated backflow design and pneumatic control makes the bioreactor physiologically capable of being studied dynamically in a 72 mm bore MRI device. Using a combination of non-degradable scaffolds and cell carrier hydrogels, we have shown a high cell density of the heart valve, confirmed by immunohistology. Consequently, our imaging approach and bioreactor design have the potential to greatly enhance quality control during the crucial transition from advanced in vitro bioreactor maturation to the initial in vivo implantation of cardiovascular implants. Ultimately, this work could contribute significantly to advancing clinical applications and improving patient safety.

Supplementary Information The online version contains supplementary material available at <https://doi.org/10.1007/s10439-024-03632-8>.

Acknowledgements This work was supported by the German Research Foundation in the Package Proposals PAK 961 (DFG—Project number:403039938).

Author Contributions Conceptualization: Saurav Ranjan Mohapatra, Fabian Kiessling, Stefan Jockenhoevel; methodology: Saurav Ranjan Mohapatra, Elena Rama, Maximilian P. Werner, Tobais Call, Tanja Loewenberg, Alexander Loewen; formal analysis and investigation: Saurav Ranjan Mohapatra, Elena Rama, Maximilian P. Werner, Tobais Call, Tanja Loewenberg, Alexander Loewen; writing—original draft preparation: Saurav Ranjan Mohapatra; writing—review and editing: Christian Apel, Elena Rama, Fabian Kiessling, Stefan Jockenhoevel; funding acquisition: Christian Apel, Fabian Kiessling, Stefan Jockenhoevel; resources: Christian Apel, Fabian Kiessling, Stefan Jockenhoevel; supervision: Christian Apel, Fabian Kiessling, Stefan Jockenhoevel. All authors have read and agreed to the published version of the manuscript.

Funding Open Access funding enabled and organized by Projekt DEAL. This work was supported by Deutsche Forschungsgemeinschaft, 403039938, Stefan Jockenhoevel

Declarations

Conflict of Interest The authors declare no conflict of interest.

Ethical Approval The umbilical cords were collected from the Gynecology Department at the University Hospital Aachen in accordance with the human subjects' approval of the ethics committee (vote of the local ethics committee: 'EK 2067').

Open Access This article is licensed under a Creative Commons Attribution 4.0 International License, which permits use, sharing, adaptation, distribution and reproduction in any medium or format, as long as you give appropriate credit to the original author(s) and the source, provide a link to the Creative Commons licence, and indicate if changes were made. The images or other third party material in this article are included in the article's Creative Commons licence, unless indicated otherwise in a credit line to the material. If material is not included in the article's Creative Commons licence and your intended use is not permitted by statutory regulation or exceeds the permitted use, you will need to obtain permission directly from the copyright holder. To view a copy of this licence, visit <http://creativecommons.org/licenses/by/4.0/>.

References

1. Claessen, B. E., et al. Considerations for Optimal device selection in transcatheter aortic valve replacement: a review. *JAMA Cardiol.* 6(1):102–112, 2021.
2. Warraich, N., et al. Long-term outcomes of mechanical versus bioprosthetic aortic valve replacement in patients aged under 50 years: meta-analysis of reconstructed time-to-event data. *Am. J. Cardiol.* 227:11–17, 2024.
3. Aluru, J. S., et al. Valvular heart disease epidemiology. *Med. Sci. (Basel)*. 10(2):32, 2022.
4. Simon, L. R., and K. S. Masters. Disease-inspired tissue engineering: investigation of cardiovascular pathologies. *ACS Biomater. Sci. Eng.* 6(5):2518–2532, 2020.
5. Namiri, M., et al. Engineering natural heart valves: possibilities and challenges. *J. Tissue Eng. Regen. Med.* 11(5):1675–1683, 2017.
6. Boroumand, S., et al. Heart valve tissue engineering: an overview of heart valve decellularization processes. *Regen. Med.* 13(1):41–54, 2018.
7. Cawley, P. J., J. H. Maki, and C. M. Otto. Cardiovascular magnetic resonance imaging for valvular heart disease: technique and validation. *Circulation.* 119(3):468–478, 2009.
8. Kramer, H., K. Nikolaou, and M. F. Reiser. Cardiovascular whole-body MRI. *Eur. J. Radiol.* 70(3):418–423, 2009.
9. Wolf, F., et al. MR and PET-CT monitoring of tissue-engineered vascular grafts in the ovine carotid artery. *Biomaterials.* 216:119228, 2019.
10. Rama, E., et al. Monitoring the remodeling of biohybrid tissue-engineered vascular grafts by multimodal molecular imaging. *Adv. Sci. (Weinh.)* 9(10):e2105783, 2022.
11. Mohapatra, S. R., et al. From in vitro to perioperative vascular tissue engineering: shortening production time by traceable textile-reinforcement. *Tissue Eng. Regen. Med.* 19(6):1169–1184, 2022.
12. Gallagher, F. A. An introduction to functional and molecular imaging with MRI. *Clin. Radiol.* 65(7):557–566, 2010.
13. Zoghbi, W. A., et al. Recommendations for noninvasive evaluation of native valvular regurgitation: a report from the american society of echocardiography developed in collaboration with the society for cardiovascular magnetic resonance. *J. Am. Soc. Echocardiogr.* 30(4):303–371, 2017.
14. Rajani, R., et al. Multimodality imaging of heart valve disease. *Arq. Bras. Cardiol.* 103(3):251–263, 2014.
15. Lichtenberg, A., et al. In vitro re-endothelialization of detergent decellularized heart valves under simulated physiological dynamic conditions. *Biomaterials.* 27(23):4221–4229, 2006.
16. Converse, G. L., et al. Design and efficacy of a single-use bioreactor for heart valve tissue engineering. *J. Biomed. Mater. Res. Part B: Appl. Biomater.* 105(2):249–259, 2017.

17. Berry, J. L., et al. Bioreactors for development of tissue engineered heart valves. *Ann. Biomed. Eng.* 38(11):3272–3279, 2010.
18. Rath, S., et al. Differentiation and distribution of marrow stem cells in flex-flow environments demonstrate support of the valvular phenotype. *PLOS ONE*. 10(11):e0141802, 2015.
19. Schenke-Layland, K., et al. Complete dynamic repopulation of decellularized heart valves by application of defined physical signals—an in vitro study. *Cardiovasc. Res.* 60(3):497–509, 2003.
20. Mol, A., et al. Tissue engineering of human heart valve leaflets: a novel bioreactor for a strain-based conditioning approach. *Ann. Biomed. Eng.* 33(12):1778–1788, 2005.
21. Karim, N., K. Golz, and A. Bader. The cardiovascular tissue-reactor: a novel device for the engineering of heart valves. *Artif. Organs*. 30(10):809–814, 2006.
22. Tefft, B. J., et al. Cardiac valve bioreactor for physiological conditioning and hydrodynamic performance assessment. *Cardiovasc. Eng. Technol.* 10(1):80–94, 2019.
23. Syedain, Z. H., and R. T. Tranquillo. Controlled cyclic stretch bioreactor for tissue-engineered heart valves. *Biomaterials*. 30(25):4078–4084, 2009.
24. Voß, K., et al. Towards technically controlled bioreactor maturation of tissue-engineered heart valves. *Biomed. Tech. (Berl)*. 67(6):461–470, 2022.
25. Zeltinger, J., et al. Development and characterization of tissue-engineered aortic valves. *Tissue Eng.* 7(1):9–22, 2001.
26. Hoerstrup, S. P., et al. New pulsatile bioreactor for in vitro formation of tissue engineered heart valves. *Tissue Eng.* 6(1):75–79, 2000.
27. Götestrand, S., et al. Visualization of wrist anatomy—a comparison between 7T and 3T MRI. *Eur. Radiol.* 32(2):1362–1370, 2022.
28. Maruyama, S., et al. Comparison of 3T and 7T MRI for the visualization of globus pallidus sub-segments. *Sci. Rep.* 9(1):18357, 2019.
29. Moreira, R., et al. Tissue-engineered heart valve with a tubular leaflet design for minimally invasive transcatheter implantation. *Tissue Eng. Part C Methods*. 21(6):530–540, 2015.
30. Dadfar, S. M., et al. Size-isolation of superparamagnetic iron oxide nanoparticles improves MRI, MPI and hyperthermia performance. *J. Nanobiotechnol.* 18(1):22, 2020.
31. Rama, E., et al. Monitoring the remodeling of biohybrid tissue-engineered vascular grafts by multimodal molecular imaging. *Adv. Sci.* 9(10):2105783, 2022.
32. Rama, E., et al. In vitro and in vivo evaluation of biohybrid tissue-engineered vascular grafts with transformative 1H/19F MRI traceable scaffolds. *Biomaterials*. 311:122669, 2024.
33. Koch, S., et al. Tissue engineering: selecting the optimal fixative for immunohistochemistry. *Tissue Eng. Part C Methods*. 18(12):976–983, 2012.
34. Amadeo, F., et al. Aortic valve cell seeding into decellularized animal pericardium by perfusion-assisted bioreactor. *J. Tissue Eng. Regen. Med.* 12(6):1481–1493, 2018.
35. Ott, H. C., et al. Perfusion-decellularized matrix: using nature's platform to engineer a bioartificial heart. *Nat. Med.* 14(2):213–221, 2008.
36. VeDepo, M. C., et al. Non-physiologic bioreactor processing conditions for heart valve tissue engineering. *Cardiovasc. Eng. Technol.* 10(4):628–637, 2019.
37. Çaykara, T., et al. Exploring the potential of polyethylene terephthalate in the design of antibacterial surfaces. *Med. Microbiol. Immunol.* 209(3):363–372, 2020.
38. Mirakabad, S. T., et al. PLGA-based nanoparticles as cancer drug delivery systems. *Asian Pac. J. Cancer Prev.* 15(2):517–535, 2014.
39. Guo, X., et al. PLGA-based micro/nanoparticles: an overview of their applications in respiratory diseases. *Int J Mol Sci.* 24(5):433, 2023.
40. Bazgir, M., et al. Degradation and characterisation of electrospun polycaprolactone (PCL) and poly(lactic-co-glycolic acid) (PLGA) scaffolds for vascular tissue engineering. *Mater. (Basel)*. 14(17):4773, 2021.
41. Jung, J. J., F. Jadbabaie, and M. M. Sadeghi. Molecular imaging of calcific aortic valve disease. *J. Nucl. Cardiol.* 25(4):1148–1155, 2018.
42. Miller, D.J., et al., *Development of a pulsatile-flow tissue engineered heart. Valve bioreactor system to mimic the physiological function of the human left heart*. In: Proceedings of the Second Joint 24th Annual Conference and the Annual Fall Meeting of the Biomedical Engineering Society Engineering in Medicine and Biology, vol.1, 2002, pp. 835–836.
43. Beelen, M. J., P. E. Neerincx, and M. J. G. van de Molengraft. Control of an air pressure actuated disposable bioreactor for cultivating heart valves. *Mechatronics*. 21(8):1288–1297, 2011.
44. Cruz, G., et al. Cardiac Magnetic resonance fingerprinting: technical developments and initial clinical validation. *Curr. Cardiol. Rep.* 21(9):91, 2019.
45. Moroz, J., and S. A. Reinsberg. Dynamic contrast-enhanced. In: *Preclinical MRI Methods and Protocols*, edited by M. L. García, and P. L. Larrubia. New York: Springer, 2018, pp. 71–87.
46. Pibarot, P., and J. G. Dumesnil. New concepts in valvular hemodynamics: implications for diagnosis and treatment of aortic stenosis. *Can. J. Cardiol.* 23:40B–47B, 2007.
47. Okura, H., et al. Planimetry and transthoracic two-dimensional echocardiography in noninvasive assessment of aortic valve area in patients with valvular aortic stenosis. *J. Am. College Cardiol.* 30(3):753–759, 1997.
48. Firstenberg, M. S., et al. Short-term hemodynamic performance of the mitral Carpentier–Edwards PERIMOUNT pericardial valve. *Ann Thorac. Surg.* 71(5):S285–S288, 2001.
49. Amarelli, C., et al. Left ventricular mass regression after aortic valve replacement with 17-mm St Jude Medical mechanical prostheses in isolated aortic stenosis. *J. Thorac. Cardiovas. Surg.* 129(3):512–517, 2005.
50. Buchanan, G., et al. TCT-843 transcatheter aortic valve implantation with edwards SAPIEN XT™ versus medtronic corevalve revalving system® with AccuTrak™: the sapere pilot study. *J. Am. Coll. Cardiol.* 60(17):B245–B245, 2012.
51. Baumgartner, H., et al. Recommendations on the echocardiographic assessment of aortic valve stenosis: a focused update from the european association of cardiovascular imaging and the american society of echocardiography. *J. Am. Soc. Echocardiogr.* 30(4):372–392, 2017.
52. Hurtado-Aguilar, L. G., et al. Ultrasound for in vitro, noninvasive real-time monitoring and evaluation of tissue-engineered heart valves. *Tissue Eng. Part C: Methods*. 22(10):974–981, 2016.
53. Kreitz, S., et al. Nondestructive method to evaluate the collagen content of fibrin-based tissue engineered structures via ultrasound. *Tissue Eng. Part C: Methods*. 17(10):1021–1026, 2011.

Publisher's Note Springer Nature remains neutral with regard to jurisdictional claims in published maps and institutional affiliations.

Supplementary data:

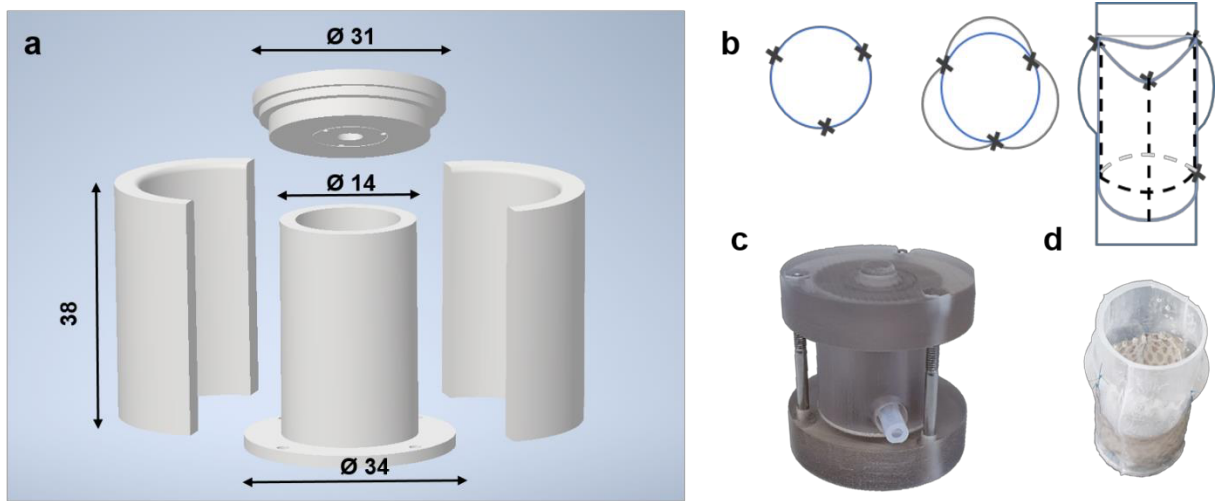


Figure S1: The mold and suturing of the heart valve: a) CAD images of different parts of the mold b) Suture points of the heart valve with the silicon housing c) The mold after 3D printed and fastened d) The heart valve inside a silicon housing after suture

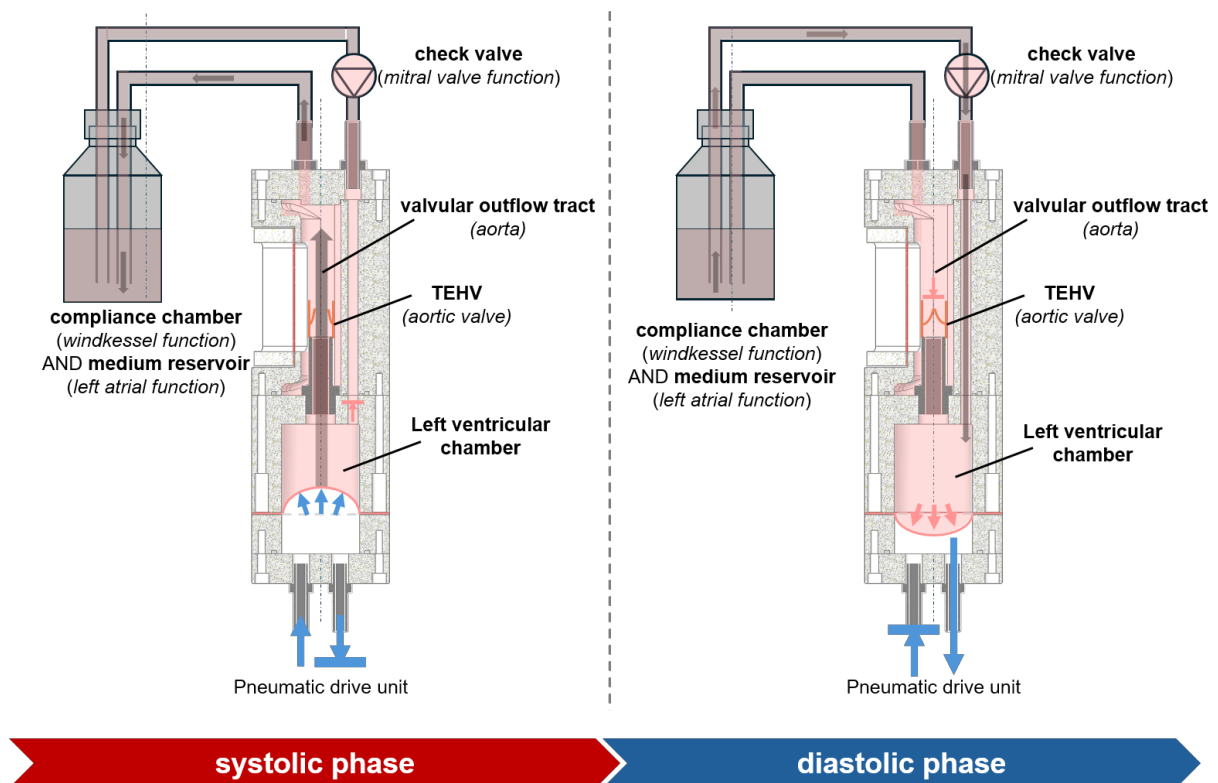


Figure S2: Principles of the bioreactor function in systolic phase and diastolic phase

Acknowledgment

I would like to express my gratitude to my supervisor, Apl. Prof. Dr. med. dent. Christian Apel, for his invaluable guidance and support throughout my doctoral thesis. His mentorship has been instrumental in shaping my research. I am also sincerely thankful to Univ. Prof. Dr. med. Stefan Jockenhoevel for his continuous encouragement and direction during my time at the institute.

My heartfelt thanks go to Ms. Elena Rama and Univ. Prof. Dr. med. Fabian Kiessling for their valuable collaboration and knowledge on noninvasive imaging and animal trials.

Special thanks to my colleagues, Mr. Tobias Call, Mr. Lukas Kellner, and Mrs. Tanja Löwenberg, for their support in the experiments. I also enjoyed sharing both work and leisure moments with my colleagues, who have become friends for life: Mrs. Stavroula Kyriakou, Mr. Yong Xu, Mr. Alp Sarisoy, Mrs. Gabriella Fois, Mrs. Selina Sonntag, and Mrs. Sabine Keutmann, who kept my spirits high.

I am thankful to my coauthors, Prof. Andrij Pich, Mrs. Miriam Alenzy Ulbrich, Mr. Christoph Melcher, and Mr. Alexander Löwen, for their insights and cooperation. My thanks also go to Mrs. Irina Apel for assistance with immunohistology and to Mrs. Julia Wolf for her overall support in the lab.

I am profoundly grateful to my family: my father, Mr. Madhusudan Mohapatra; my mother, Mrs. Ratnaparava Sahoo; and my brother, Dr. Saubhagya Ranjan Mohapatra, whose unwavering support, love, and belief in me have been the foundation of this journey.

Finally, I am especially grateful to Alina, the love of my life, for her constant encouragement and for making every step of this path more meaningful.

Affidavit according to § 5 (1) for Data Retention

Hiermit erkläre ich, dass die dieser Dissertation zu Grunde liegenden Originaldaten (I hereby declare that the original data forming the basis of this doctoral thesis are stored) im Institut für Angewandte Medizintechnik, NRW Schwerpunktprofessur Biohybrid & Medical Textiles, Forckenbeckstraße 55, 52074 Aachen hinterlegt sind.

Affidavit according to § 5 (1) and (2), and § 11 (3) 12 of the doctoral studies regulations

I, Saurav Ranjan Mohapatra, hereby declare on oath, that I have contributed a significant part, and thus majority, of the publication:

S. R. Mohapatra, E. Rama, C. Melcher, T. Call, M. A. Enezy-Ulbrich, A. Pich, C. Apel, F. Kiessling & S. Jockenhoevel: From In Vitro to Perioperative Vascular Tissue Engineering: Shortening Production Time by Traceable Textile-Reinforcement; Tissue Engineering and Regenerative Medicine; 2022, Volume 19, Pages 1169–1184.

The contributions to the publication were as follows:

Names ->	S. R. Mohapatra	E. Rama	C. Melcher	T. Call	M. A. Enezy-Ulbrich	A. Pich	F. Kiessling	S. Jockenhoevel	C. Apel	Sum (%)
Study supervision						10	30	30	30	100
Study design/conception	20					10	25	25	20	100
Sample preparation	70	10	5	10	5					100
In vitro MRI	40	40					10	10		100
Data analysis	70	20		10						100
Scaffold production and electrospinning	50		30	20						100
Hydrogel and copolymer preparation	60			10	30					100
Performing experiments	70	15	5	10						100
Statistical evaluation	90	10								100
Manuscript writing	100									100
Manuscript revising		5	5	5	5	5	20	20	35	100

The position as the first author obviously arises from this significant contribution.

Saurav Ranjan Mohapatra

As supervisor and / or corresponding author I confirm the statements of Saurav Ranjan Mohapatra and as a representative of the collaborative partners

Christian Apel
Doctoral supervisor

Stefan Jockenhoevel
Corresponding author

As co-author I endorse the statement of Christian Apel

E. Rama

C. Melcher

T. Call

M. A. Enezy-Ulbrich

A. Pich

F. Kiessling

Affidavit according to § 5 (1) and (2), and § 11 (3) 12 of the doctoral studies regulations

I, Saurav Ranjan Mohapatra, hereby declare on oath, that I have contributed a significant part, and thus majority, of the publication:

S. R. Mohapatra, E. Rama, M. P. Werner, T. Call, T. Loewenberg, A. Loewen, C. Apel, F. Kiessling & S. Jockenhoevel: Novel Bioreactor Design for Non-invasive Longitudinal Monitoring of Tissue-Engineered Heart Valves in 7T MRI and Ultrasound; Annals of Biomedical Engineering; 2024.

The contributions to the publication were as follows:

Names -->	S. R. Mohapatra	E. Rama	M. P. Werner	T. Call	T. Loewenberg	A. Loewen	F. Kiessling	S. Jockenhoevel	C. Apel	Sum (%)
Study supervision							30	30	40	100
Study design/conception	30						20	30	20	100
In vitro MRI	40	40		10	10					100
Sample preparation	60	5	5	10	10	10				100
Scaffold production and electrospinning	60			5	5	30				100
Data analysis	80	10	5		5					100
Performing experiments	70	10		10	10					100
Statistical evaluation	90	5			5					100
Manuscript writing	100									100
Manuscript revising		5	5	5	5	5	20	20	35	100

The position as the first author obviously arises from this significant contribution.

Saurav Ranjan Mohapatra

As supervisor and / or corresponding author I confirm the statements of Saurav Ranjan Mohapatra and as a representative of the collaborative partners

Christian Apel
Doctoral supervisor

Stefan Jockenhoevel
Corresponding author

As co-author I endorse the statement of Christian Apel

E. Rama

M. P. Werner

T. Call

T. Loewenberg

A. Loewen

F. Kiessling



SAURAV RANJAN MOHAPATRA

Address: Augustastraße 49, 52070 Aachen
Email: mohapatra@gmx.de
Phone: +49 17622676369
Date of Birth: 15.06.1993
Place of birth: Kendupalli, India
Nationality: Indian

EDUCATION

Doctoral Studies

RWTH Aachen University, Germany

Doctorate (Dr. rer. medic.)
at the Institute of Applied Medical Engineering (AME)
November 2019 – present (expected 2025)

Master of Science

UNIVERSITY OF BAYREUTH, GERMANY

Master of Science in Biofabrication
April 2017- April 2019

Bachelor of technology

BIJU PATANAIAK UNIVERSITY OF TECHNOLOGY, ODISHA, INDIA

Bachelor of technology in Mechanical engineering
August 2010- September 2014

EXPERIENCE

Research Assistant

At Institute of Applied Medical Engineering (AME), RWTH Aachen.
(since 1st November 2019)

Main Projects:

- Development and conditioning of tissue-engineered vascular graft and their monitorability via non-invasive imaging
- Design and development of bioreactor for tissue-engineered heart valves suitable for 7T MRI

Master thesis

“4D Biofabrication using shape-changing hydrogels”
at Ionov-Lab University of Bayreuth (July 2018- April 2019)

Work experience

Student job (Hi Wi) at the department of production technique,
university of Bayreuth (Oct-Dec 2018)

INTERNSHIP

- Computer aided design (CATIA v5) training at central toolroom and training center, Bhubaneswar, India (Sep-2013)
- Vocational training at Tata motors, Bhubaneswar, India (Aug-2012)
- Industrial internship at Hindustan Aeronautics limited, Koraput, India (Aug- 2013)

INTERESTS

- Badminton
- Writing
- Cooking
- Travelling

LANGUAGES

- English (Full proficiency)
- German (Intermediate proficiency, B1)
- Hindi (Native)
- Odia (Native)